CFD Investigation of the Aerodynamic Support Interference of a Semi-Span Model Equipped with a T-tail

Mahmoud Mamou and Cabot Broughton
Aerodynamics Laboratory
Aerospace Research Centre, National Research Council Canada
1200 Montreal Rd, Ottawa, Ontario, K1A 0R6
CANADA

mahmoud.mamou@nrc-cnrc.gc.ca

ABSTRACT

High-fidelity CFD flow simulations were carried out to assess the sources of aerodynamic support interference of an aircraft half-model with a T-tail empennage mounted in a wind tunnel in an attempt to improve how well a semi-span model can represent the corresponding full-span aircraft. The Bombardier Research Aircraft Configuration (BRAC) model was used, which consists of a fuselage, a fuselage to wing fairing, a cruise wing with flap fairings, an engine nacelle and pylon, a vertical tail and a horizontal stabilizer (HStab). The standard half-model support used at the National Research Council Canada consists of a wall mounted splitter plate to remove a sizable portion of the upstream tunnel wall boundary layer and a two-dimensional peniche sandwiched between the model symmetry plane and the splitter plate. Using unstructured grid topology with adequate surface and volume grid distributions, CFD simulations of the BRAC model mounted in the wind tunnel were performed using the Menter Shear Stress Transport turbulence model. All the flow solutions were obtained for subsonic flight conditions at a Mach number of 0.2. The CFD results for the standard (Baseline) mounting arrangement compared favourably with half-model experimental wind tunnel data. The BRAC CFD model was then modified to provide reference "full-span" data, and to examine several alternate model mounting arrangements. All simulations were compared with the ideal full-span reference simulations. Significant disturbances were found to be induced by the reflection plane primary horseshoe vortex on the flow field surrounding the HStab, which had a direct impact on the measured overall model forces and moments.

1.0 INTRODUCTION

Half-model aircraft testing at the National Research Council Canada (NRC) 1.5 m trisonic wind tunnel has been used extensively by the aerospace industry, such as Bombardier Aviation (BA), for the development of regional jets, business jets and regional turboprops. The design of a wind tunnel half-model for a conventional aircraft, where only a wing-body or a wing-body with a fuselage-mounted horizontal stabilizer (HStab) is represented, is fairly well established. In both of these cases, the vertical tail fin is not represented by the model. When installed in the wind tunnel test section, the model is usually offset from the tunnel wall or splitter plate by a non-metric spacer shaped as a two-dimensional extrusion of the centreline outline of the model. This component is called a boundary layer filler plate or a peniche, and it is implemented to reduce the interference effects of the reflection plane boundary layer flows on the model aerodynamic loads. However, when an aircraft with a "T" tail is tested in a half-model configuration and it is desired to obtain experimental data for the performance of the horizontal stabilizer (HStab), the vertical tail assembly must be included on the model. Extension of the typical boundary layer filler plate method outlined above to a vertical tail is a simple and common methodology; however, from an aerodynamic perspective, it is apparent

that this method could produce large interferences in the region of the empennage, complicating the application of the half-model test results as representative of the full-span equivalent.

A large number of previous studies have examined wind tunnel testing practices that can be used to reduce interference from the test section reflection plane boundary layer during semi-span aircraft model testing. A few of these are described below.

To support the development of semi-span aircraft model (without empennage) testing capabilities at NASA Langley Research Center's National Transonic Facility, Milholen and Chokani [1] performed a computational investigation of advanced subsonic transport aircraft testing at full-scale Reynolds numbers. A Navier-Stokes solver was used to simulate the flow and examine methods to streamline the flow past a semi-span aircraft configuration mounted with a standoff peniche. It was demonstrated that the aerodynamic performance of a semi-span configuration could be improved by decreasing the peniche thickness. The best peniche thickness was found to be equal to twice the tunnel-empty sidewall boundary layer displacement thickness; this allowed the tunnel to reproduce the aerodynamic characteristics of the full-span configuration reasonably well. Blowing jets placed on the sidewall/peniche juncture region were found to reduce the wall boundary layer effect and improve the flow over the aft region of the semi-span model.

Doerffer and Szulc [2] performed flow simulations past the DLR F11 model in the European Transonic Wind Tunnel using full-span and half-span models with and without a 30-mm-thick peniche configuration, for both low and high angles of attack. The DLR F11 model was not equipped with a vertical tail and empennage; thus wall interference was not significant. The authors were surprised to find that in comparison with the experiment, the best match with full-span data was obtained for a model mounted directly on the wall, without the addition of a peniche. This was the case because the model did not include a tail, so the induced horseshoe vortex did not interact anywhere with the aircraft structure and its effect was very weak.

Eder et al. [3] investigated the difference between results obtained using full-span and semi-span models. The aircraft model was a 2.28-m-long wing-fuselage combination without a tail assembly. The main objective of their investigation was to assess the effect of the peniche on the aerodynamic coefficients. Their numerical and experimental studies showed that the deviation between full-span and semi-span aerodynamic coefficients increased with increasing peniche thickness. It was observed that the horseshoe vortex that developed on the wall in front of the 2D peniche had a significant influence on the flow around the model. Further results showed that it was beneficial to remove the peniche and leave a gap between the model and the wind tunnel wall. The optimal gap size was found to be about four times the displacement thickness of the tunnel wall boundary layer in front of the fuselage.

Yokokawa et al. [4] conducted a series of wind tunnel experiments using the Jaxa high-lift configuration Standard Model (JSM) as part of a research program to improve the aerodynamic design methodology for an efficient aircraft high-lift system in the JAXA-LWT1 wind tunnel. The aircraft model consisted of a wing, a fuselage, leading-edge slats, flaps, a nacelle-pylon, slat tracks and flap fairings. The model was not equipped with a tail. Different peniche thicknesses were considered in an attempt to reduce the tunnel wall boundary layer interference. A numerical investigation was performed to determine the desirable height of the peniche by comparing computational results of the full-span model in free-flight condition to the half-span model modelled using a non-slip wall boundary condition. The optimal peniche height was found to be approximately two to three times the displacement thickness (30 mm) of the tunnel wall boundary layer. For reference, their boundary layer thickness was 150 mm.

Skinner and Zare-Behtash [5] performed an experimental investigation on a semi-span wind tunnel model without a tail at several stand-off gap heights without using a peniche. Their investigation was supported by PIV measurements and flow visualisation, which provided the flow behaviour around the aircraft model. The tested stand-off gap height was varied from 1.5 to 5 times the wind tunnel boundary layer displacement thickness. The aerodynamic flow behaviour and characterisation suggested that semi-span model testing

without a peniche led to more natural results/flow fields than what would be achieved with a 2D-peniche. It was also observed that a peniche extrusion generated a horseshoe vortex in front of the fuselage at the wall juncture, which influenced the flow over the fuselage and the inboard wing.

As part of a large collaborative project, Lockheed Martin, the Air Force Research Laboratory and NASA teamed up for a first-of-its-kind wind tunnel validation effort using a hybrid wing body (HWB) next-generation airlifter at the National Transonic Facility (NTF). Chan et al. [6] and Wick et al. [7] documented some of the project work that was achieved as of 2017. The semi-span HWB model consisted of a blended high-aspect-ratio swept wing with a lifting forebody and a standard aft fuselage and T-tail empennage. The model also consisted of an over- or under-wing nacelle. A nonmetric peniche was used to offset the model from the tunnel sidewall. The model standoff from the wall, including the peniche thickness, was 50.8 mm, which is the common practice for semi-span high-lift tests at the NTF facility. A gap was created between the vertical tail centreline and the tunnel wall. The vertical tail base was designed as a flat surface to minimize channel interference effects with the sidewall; however, the vertical tail upper bullet-shaped fairing was retained to ensure sufficient material to mount the horizontal stabilizer. A 5-mm labyrinth seal gap was used between the HWB model and the peniche. The semi-span model setup methodology in the wind tunnel was considered optimal for reducing the wall interference and avoiding choking flows through the vertical tail gap.

The present paper focuses on a computational fluid dynamics (CFD) investigation of the Bombardier Research Aircraft Configuration (BRAC) half-model support interference caused by the boundary layer filler plate arrangement used in wind tunnel tests. Three practical alternate model configurations were modelled in an attempt to improve how well the vertical tail of a semi-span model represents the corresponding full-span aircraft in the wind tunnel. The alternate configurations, described in Section 3, were only modelled by CFD; no experimental data have been collected so far for these configurations.

The CFD simulations were performed using the Cobalt compressible flow solver [8] assuming fully turbulent flows, and applying the Menter Shear Stress Transport (SST) model [9]. The flow simulations were conducted on unstructured viscous grids that were generated using the Pointwise mesh generator [10]. The results are presented in terms of flow patterns (pressure, vorticity and Mach number distribution, and iso-surface vorticity) and the aerodynamic loads acting on the BRAC model.

2.0 WIND TUNNEL DESCRIPTION AND TESTING PRACTICE

The present CFD investigations considered standard testing of a half-model aircraft (BRAC) in the NRC 1.5 m trisonic blowdown wind tunnel [11]. The wind tunnel is an intermittent, open-circuit, pressurized, blowdown to atmosphere exhaust facility, with a Mach number ranging from subsonic to supersonic flow. The tunnel is supplied by an air storage volume charged to 21 atmospheres by a centrifugal air compressor. During a blowdown, the total pressure is maintained constant to within 0.5% of the set value throughout a run using a regulated control valve. The settling chamber is equipped with acoustic baffles section and damping screens to ensure flow uniformity prior to the contraction. A transonic test section surrounded by a plenum chamber are installed in the tunnel circuit, with a test section cross-section of 1.5 m × 1.5 m and length of 4.87 m, with perforations on all four walls. The perforations are 12.5-mm-diameter holes oriented at a 60^{o} angle upstream and provide a porosity of 6%. Throttle plates on the plenum side permit the open area ratio to be adjusted between 1 to 6%. For the test described in this paper, the porosity was fixed to 4% for both subsonic and transonic conditions. When testing at subsonic conditions, the four diffuser re-entry flaps are set at given positions and the Mach number value is controlled by a downstream throat. Servo-controlled choke fingers at this throat actively maintain the Mach number fluctuation within ±0.001.

For half-model aircraft tests, the standard 3D transonic test section is modified to accommodate the half-model setup with an aim to minimize model support interference. To reduce the impact of the relatively thick

wall boundary layer built up from the contraction/nozzle walls to the test section, a 3.43-m-long by 1.5-m-high by 6.4-mm-thick solid splitter plate-style reflection plane is mounted 51 mm off of the test section wall supporting the model. The 51-mm gap diverts the wall boundary layer flow behind the splitter plate. The test section wall porosity behind the splitter plate is set to 6% to vent the flow freely into the plenum and avoid choking within the gap. A new boundary layer develops on the splitter plate. The splitter plate leading edge is located 1.5 m upstream from the balance centre of rotation.

The wind tunnel balance, which is mounted on the left wall of the test section (when looking upstream), is an external six-component body axis strain-gauge balance with calibration uncertainties of 0.1% of full scale for the normal and axial forces, and the pitching moment.

The half-model setup support consists of a 25-mm-thick filler plate (peniche) sandwiched between the model symmetry plane and the reflection plane. The peniche is attached to a 610-mm-diameter turntable connected to the pitching non-metric portion of the balance. The wind tunnel model symmetry plane has a small gap to the peniche and incorporates non-contact labyrinth seals; however, in the present CFD work, this gap was sealed and treated as a solid boundary.

Although a perforated transonic test section is used for all half-model tests at this facility, a large portion of half-model testing is performed to examine high-lift aircraft configurations. Through pressurization, chord Reynolds numbers of 7.5 million can be provided for freestream Mach numbers from 0.2 to 0.9. With optimum perforated wall settings, substantially lower farfield wall interference is obtained relative to a solid wall test section of the same size.

The reference static pressure for the half-model configuration is a static tap located on the opposite wall of the splitter plate at mid-height, approximately 125 mm downstream of the splitter plate leading edge.

In the wind tunnel experiments, the data reduction corrections rely on a “1-variable” method developed by Mokry [12], which is used for farfield wall interference correction of the tunnel perforated wall boundaries. This method requires a potential flow description of the model, the uncorrected balance measurements, and the simultaneous measurement of the streamwise velocity distribution on the three farfield boundaries. The full surface velocity distributions are derived from six wall-mounted axial static pressure tubes (two tubes per wall). Each 25-mm-diameter by 4.14-m-long tube is instrumented with 32 static pressure taps distributed non-uniformly along its length from 2.285 m upstream to 1.4 m downstream of the balance axis. The primary corrections are the change in angle of attack and Mach, while the change in drag due to second-order buoyancy corrections is also computed.

3.0 BRAC MODEL DESCRIPTION

The main objective of this study was to reduce the interferences caused by the model support arrangement of the NRC 1.5m wind tunnel, and as such, the CFD simulations were performed by simulating the wind tunnel’s reflection plane boundary layer and the model with its support in a free-air farfield, without adding the complexities of simulating the three perforated farfield tunnel wall boundaries. The CFD results were compared directly to the wind tunnel data corrected for the farfield wall interference. To this end, the Bombardier Research Aircraft Configuration (BRAC) computer-aided design (CAD) model was used for the CFD, as displayed in Figure 1. The BRAC aircraft model consists of a fuselage, a fuselage to wing fairing, a cruise wing with flap fairings, an engine nacelle and pylon, a vertical tail and a horizontal stabilizer set at zero degrees incidence. The BRAC model mean aerodynamic chord was 277.9 mm. All flaps and control surfaces of the wing were merged into the main wing at zero degrees deflection. The cruise wing configuration of this model was selected to reduce the simulation complexities significantly. Experimental wind tunnel data existed for this configuration for both low-speed and cruise Mach numbers. For simplicity, only the Mach 0.2 flow condition was studied in this paper. Cruise conditions are currently under

investigation. The BRAC model engine was modelled as a solid nozzle with flow through.

The present paper focuses on a CFD investigation of the vertical tail support interference caused by a number of peniche arrangements (alternates). To perform the CFD investigation, five BRAC configurations were considered; they are described in detail in the following subsections and are summarized in Table 1 below.

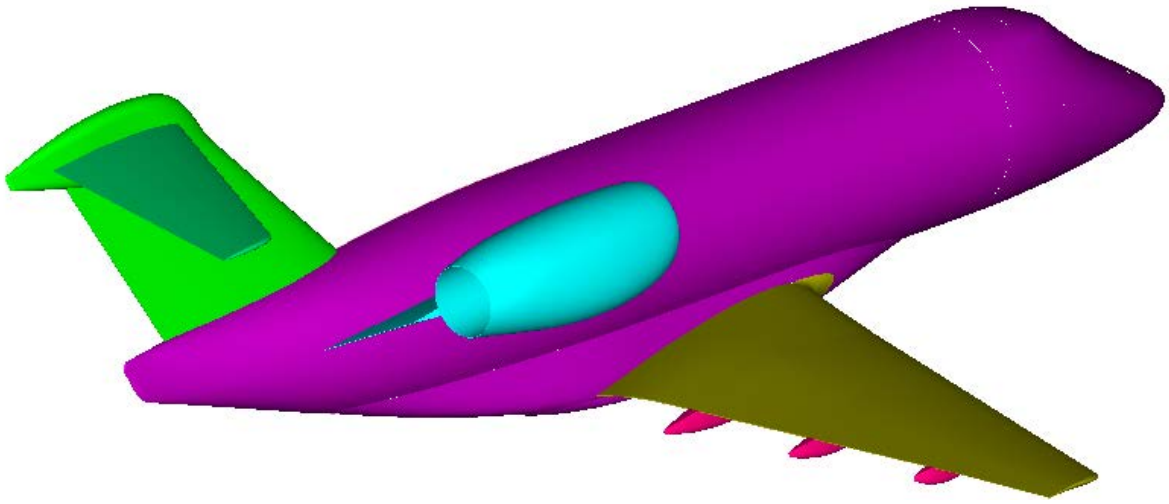

Figure 1: CAD half-model of the BRAC aircraft.

Table 1: Description of the BRAC model and alternate configurations.

Configuration	T-tail representation
Baseline	Standard BRAC half-model setup as tested at the NRC wind tunnel with a 2D peniche of the entire model centreline symmetry plane. Non-slip condition applied to the region of the wind tunnel splitter plate; slip conditions applied upstream of the splitter plate.
Reference	Theoretically perfect BRAC semi-span model with an ideal slip condition reflection plane placed at the model centreline, used to provide reference full-span data.
ALT1	Baseline BRAC configuration with a gap between the vertical tail centreline and the splitter plate. Used in an attempt to reduce the effect of forcing the reflection plane boundary layer flows and convected horseshoe vortices over the vertical fin.
ALT2	BRAC ALT1 configuration with a curved 3D peniche instead of a 2D peniche. Used in an attempt to reduce the magnitude of the convected vortices.
ALT3	BRAC ALT2 configuration with the whole vertical tail and HStab mirrored about the vertical tail centreline so that the bullet-shaped fairing at the top of the tail and the Hstab are represented. Used in an attempt to streamline the flow evenly on both sides of the vertical tail with respect to its centreline.

3.1 Baseline BRAC Model with 2D Penich

The Baseline configuration consists of the actual BRAC half-model with a full peniche. The peniche is a 2D extrusion of the model outline at the symmetry plane bridging the gap between the model centreline and the splitter plate. The thickness of the peniche is about 25 mm, as shown in Figure 2. CFD and experimental measurements have shown that the boundary layer thickness at the nose of the model is approximately 8.7 mm. There is a gap between the BRAC model symmetry line and the peniche edge in the wind tunnel experimental model that is sealed in the CFD simulations. The half-model symmetry line is slightly more than 25 mm from the splitter plate. The peniche and the sealed gap in the Baseline configuration are non-metric components.

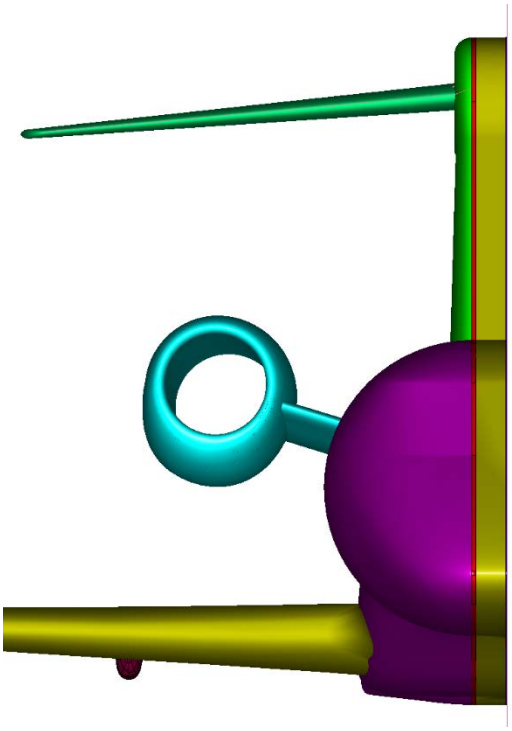

Figure 2: BRAC Baseline model with a full peniche.

3.2 Full Span BRAC Model

The BRAC Reference configuration corresponds to an ideal semi-span model aircraft, as displayed in Figure 3. In this case, slip conditions are applied to the reflection plane at the model centreline, which forms a plane of symmetry. This creates a theoretical full-span configuration that was used to obtain full-span reference data.

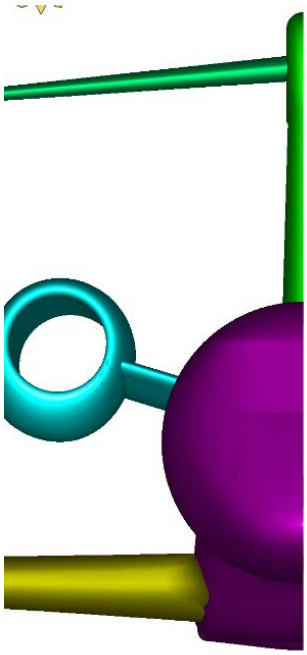

Figure 3: Semi-span BRAC model configuration.

3.3 Alternate ALT1 Configuration

The first alternate configuration (ALT1) consists of the baseline peniche of the BRAC fuselage only, with a gap between the vertical tail centreline and the splitter plate (the peniche portion of the vertical tail is removed), as shown in Figure 4. The ALT1 vertical tail design consists of a mirror image of the vertical tail about the centreline translated toward the splitter plate by the labyrinth gap distance. The mirrored CAD model of the vertical tail is then truncated at 7.62 mm from the peniche starboard edge. Therefore, the gap width between the mirrored vertical tail base and the splitter plate is 17.15 mm, whereas the boundary layer thickness at the nose of the model is approximately 8.7 mm. The mirrored vertical tail on the port side of butt-line 0 is non-metric and was included to permit a structurally practical arrangement for a future wind tunnel experimental study. This configuration was used in an attempt to reduce the interference by not forcing the entire splitter plate boundary layer flow, including the convected horseshoe vortices, out over the vertical fin.

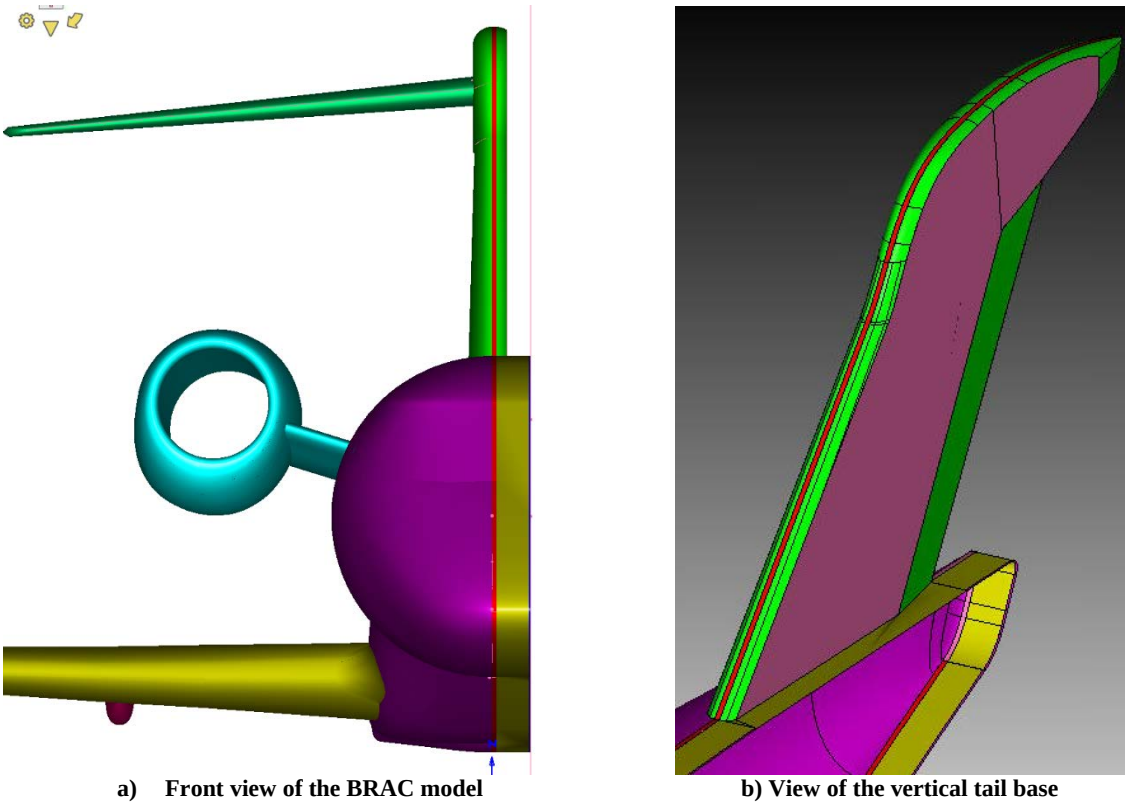

a) Front view of the BRAC model

b) View of the vertical tail base

Figure 4: BRAC model with the ALT1 configuration.

3.4 Alternate ALT2 Configuration

For this configuration, as shown in

Figure 5, the Baseline 2D peniche is removed completely and replaced by a 3D curved peniche, which was designed by making a mirror image of the BRAC fuselage and the vertical tail. Then, the mirror image of the fuselage is translated toward the splitter plate by the labyrinth gap distance, and truncated afterward right at the Teflon seal layer edge. For the vertical tail, it is truncated 7.62 mm from the peniche edge. The gap width between the vertical tail base and the splitter plate is therefore 17.145 mm. This configuration was designed in an attempt to reduce the magnitude of the convected vortices formed where the peniche nose meets the splitter plate.

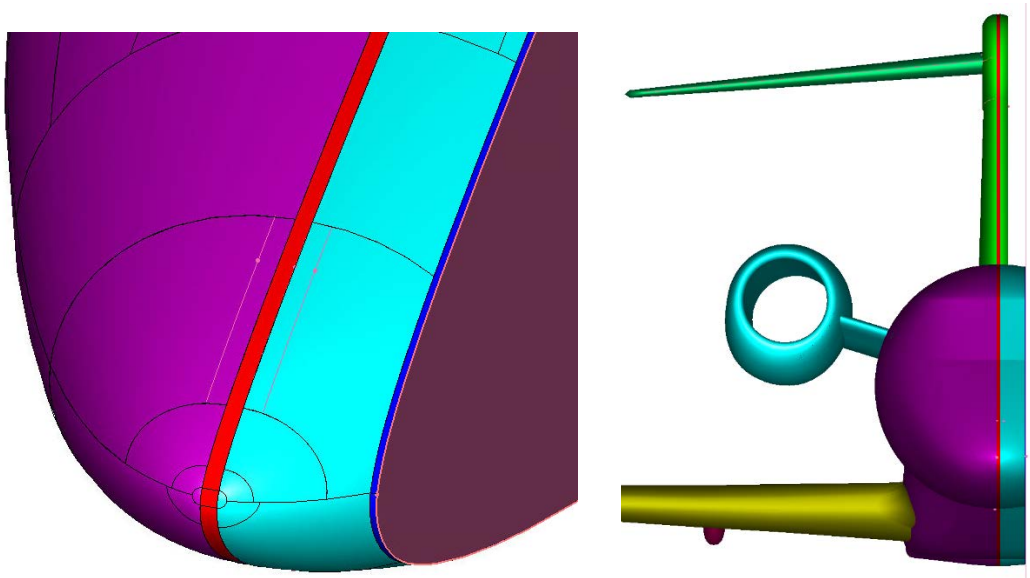

a) Front view of the BRAC model b) View of the vertical tail gap

Figure 5: BRAC model with the ALT2 configuration, with a curved peniche.

3.5 Alternate ALT3 Configuration

For the ALT3 configuration, as displayed in Figure 6, the whole vertical tail and HStab were mirrored. The mirrored HStab was chopped at the splitter plate and the mirrored vertical tail was truncated 7.6 mm from the peniche edge, while maintaining the full bullet-shaped fairing near the top of the tail. The HStab was also allowed to extend to the splitter plate. In this situation, all the mirrored parts are non-metric and isolated from the balance. This configuration was designed in an attempt to streamline the flow evenly on both sides of the vertical tail with respect to its centreline and to maintain the full span aspect ratio of the HStab.

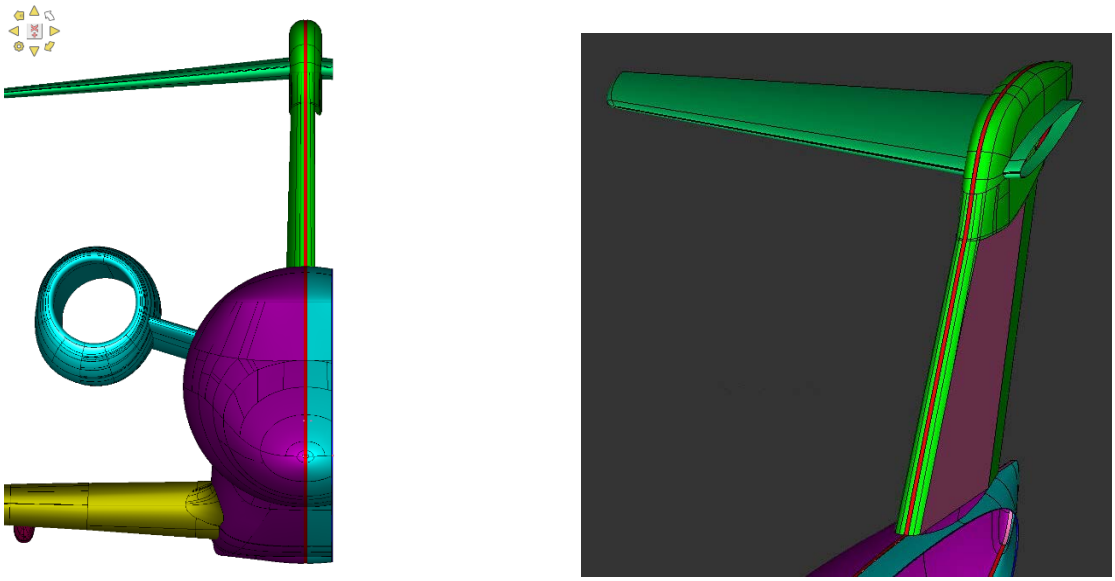

a) Front view of the BRAC model b) View of the vertical tail bullet-shaped fairing

Figure 6: BRAC model with the ALT3 configuration, with a vertical tail fairing and HStab extension.

4.0 FLOW CONDITIONS

To assess the aerodynamic interference of the various model support configurations, three angles of attack and one Mach number were considered in the current investigation. The flow conditions were those tested in the 1.5 m trisonic wind tunnel for Mach=0.2, see Table 2; note that the tunnel makes use of pressurization to increase the test Reynolds number. All the simulations were performed with free-air boundary conditions imposed at the farfield; therefore, the CFD data are compared with the corrected wind tunnel data for free-air flow conditions. At the farfield, a very weak turbulence intensity was considered, which corresponds to the default flow conditions in the Cobalt solver when using the Menter SST turbulence model. The turbulence intensity in the wind tunnel was not measured and deemed to be very low.

5.0 GRID TOPOLOGY AND SURFACE/VOLUME MESH

The BRAC model CAD geometry was imported into the Pointwise grid generator software [9]. To mesh the BRAC model and the flow field, two main mesh blocks were constructed: one block containing the BRAC model turntable and the splitter plate, and the second one extending from the inner block boundary to the farfield. As shown in Figure 7, the inner block consists of a cylinder with a hemisphere on top, both containing the BRAC model and the wind tunnel turntable. For the outer block, the farfield was located 45 m from the model. The upstream and downstream boundaries were located at 46.5 m and -43.5 m, respectively, giving a farfield at approximately 160 mean aerodynamic chords. For a given angle of attack, the BRAC model is kept at 0^o geometrical pitch angle; however, the splitter plate leading edge is tilted about the balance centre by the flow angle of attack, as demonstrated in Figure 7a. Upstream of the splitter plate leading edge, a fictitious plane is extended to the limits of the computational domain and a slip condition is applied to this plane. To simulate the wing, nacelle and HStab wakes adequately, resolution volumes, known in the Pointwise mesher as volume sources, were added within the flow fields, as shown in Figure 7b. This allowed the software to refine the grid along the wing and HStab tip vortices, near the wakes around the vertical tail leading and trailing edges, and around the bullet fairing.

Table 2: Flow conditions for Mach=0.2.

Total temperature T_0 (K)	293
Total pressure P_0 (kPa)	626.6
Static air density ρ_{REF} (kg/m^3)	7.30
Static viscosity μ_{REF} (Pa m/s)	1.80E+05
Freestream speed V_{REF} (m/s)	68.36
L_{REF} (m)	0.2779
S_{REF} (m^2)	0.2323
Re	7.7E+06
Turbulence intensity %	0.0016
eddy viscosity ratio ν_t/ν	0.001
Dissipation rate ω (s^{-1})	683.6

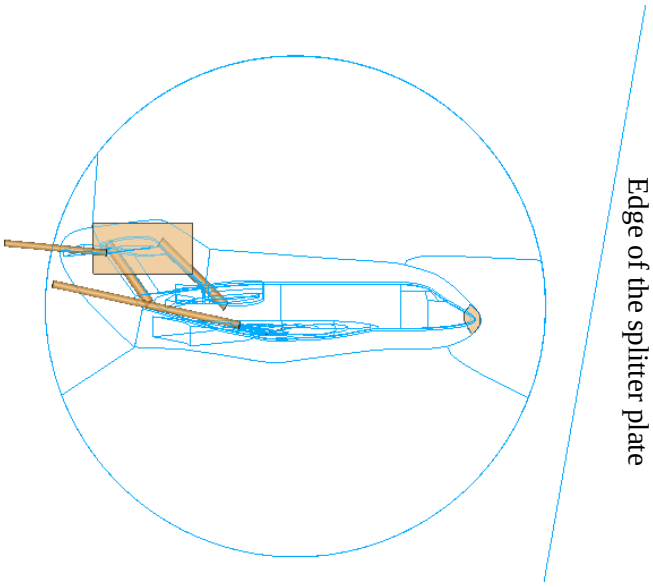

a) Inner blocks topology, side view

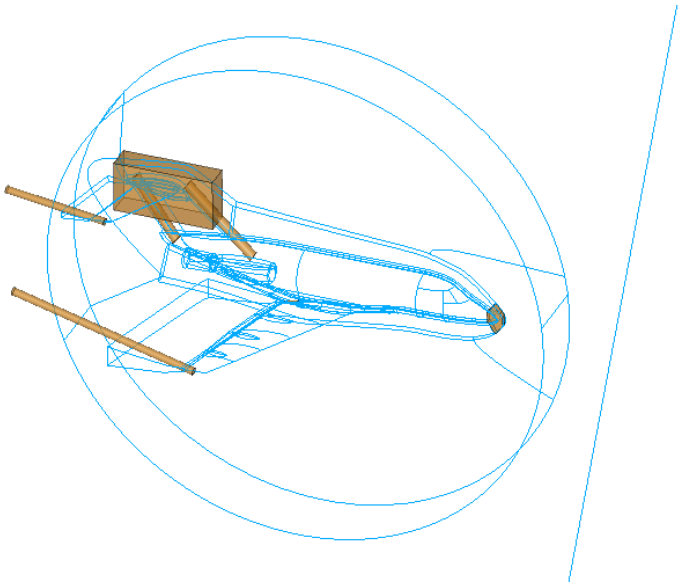

b) Inner blocks topology, isometric view

Figure 7: Grid topology around the BRAC aircraft model within the inner blocks.

For the surface grid, as displayed in Figure 8 through Figure 10, the mesh cell size was varied from 0.1 mm to 5 mm, depending on the model surface curvature, size and shape. At the wing leading edge and tip, the mesh resolution was 0.5 mm, and at the trailing edge it was 0.2 mm. On the HStab, a resolution of 0.125 to 0.15 mm was considered at the leading and trailing edges respectively. At the upstream edge of the splitter plate, as shown in Figure 8a, a resolution of 0.1 mm was considered. On the boundary of the inner blocks, the mesh size was varied from 10^{-3} mm on the splitter plate to 50 mm elsewhere off the model. The grid resolution on the outer block boundaries at the farfield was 2 m. Figure 8a shows the grid density around the BRAC model on the splitter plate, while Figure 8b illustrates the grid distribution used in the close vicinity of the fuselage/peniche nose. Figure 9 shows the surface grid distribution on the BRAC model with a close-up view on the vertical tail assembly, where more grid refinement was

performed to capture the horseshoe vortex interaction with the vertical tail.

The volume mesh was generated using the TRex algorithm in the Pointwise software considering a viscous grid topology. TRex allowed the generation of prism layers on the viscous walls using a growth rate of 1.2, with the first cell vertex from the wall fixed at 10^{-6} m. The off-wall spacing was chosen adequately to ensure a y^+ close to unity. The volume mesh distribution on a cutting plane through the BRAC model is displayed in Figure 10, where the prism layers are visible. The figure also shows the dense grid across the anticipated horseshoe vortex location. The mesh size varied from about 100 million to 140 million cells, depending on the alternate vertical tail configuration being modelled. The volume mesh consisted of prisms, hexas, tetras and pyramids.

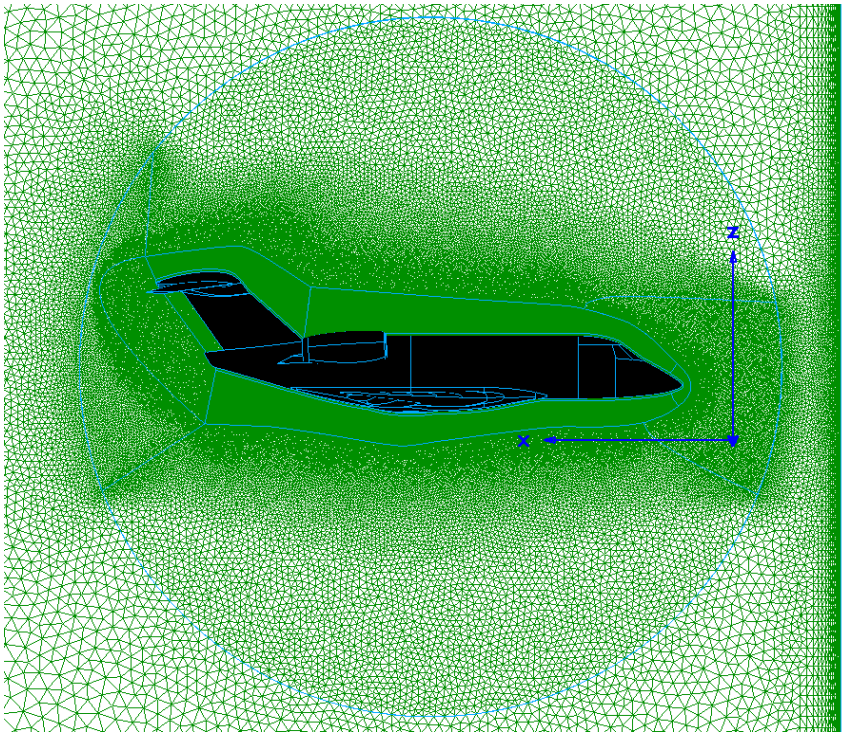

a)

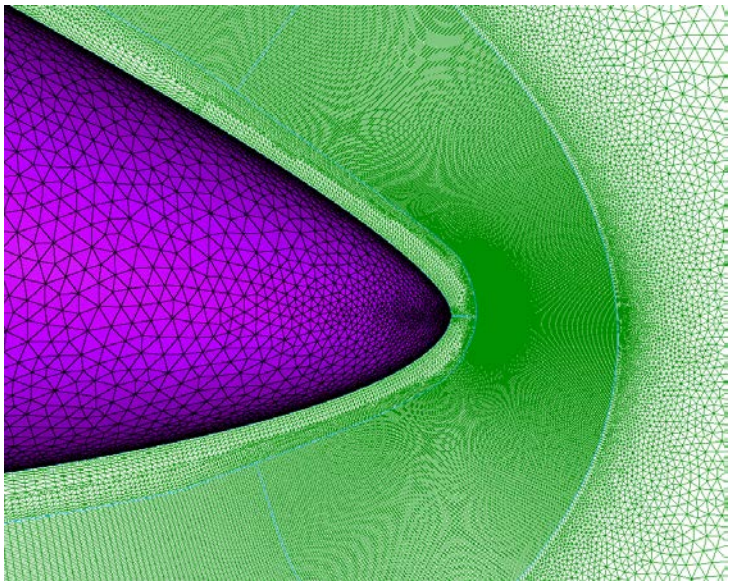

b)

Figure 8: Surface mesh distribution on the BRAC aircraft CAD model and splitter plate.

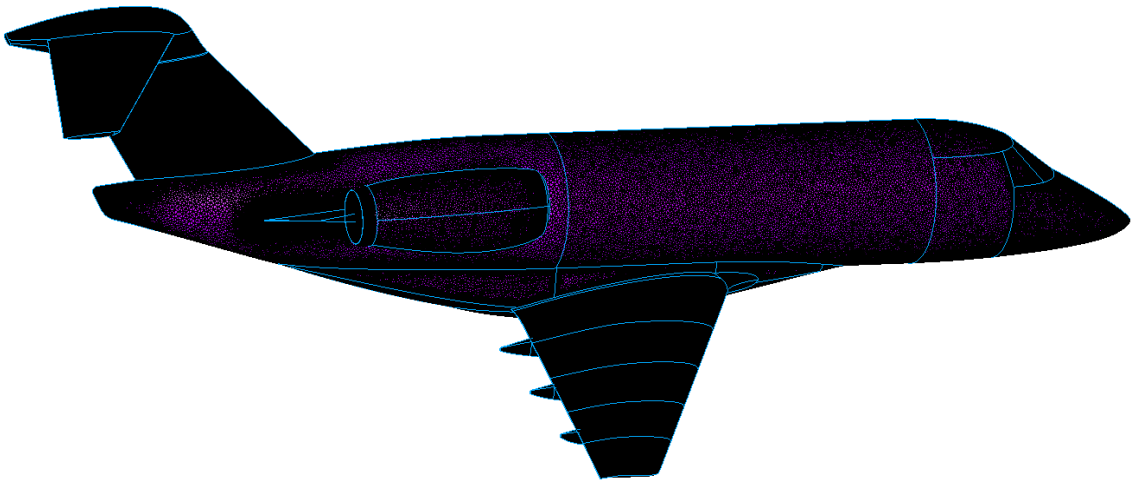

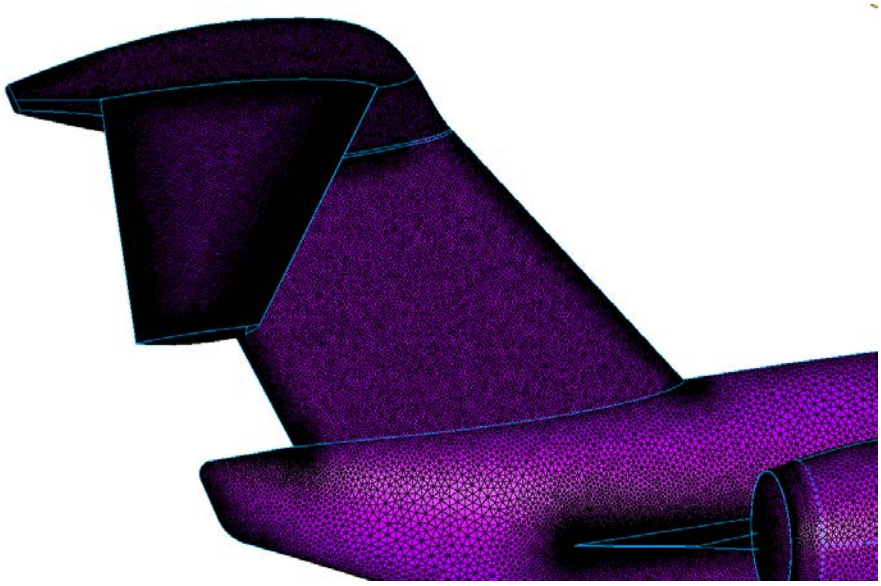

Figure 9: Surface mesh distribution on the BRAC aircraft CAD model.

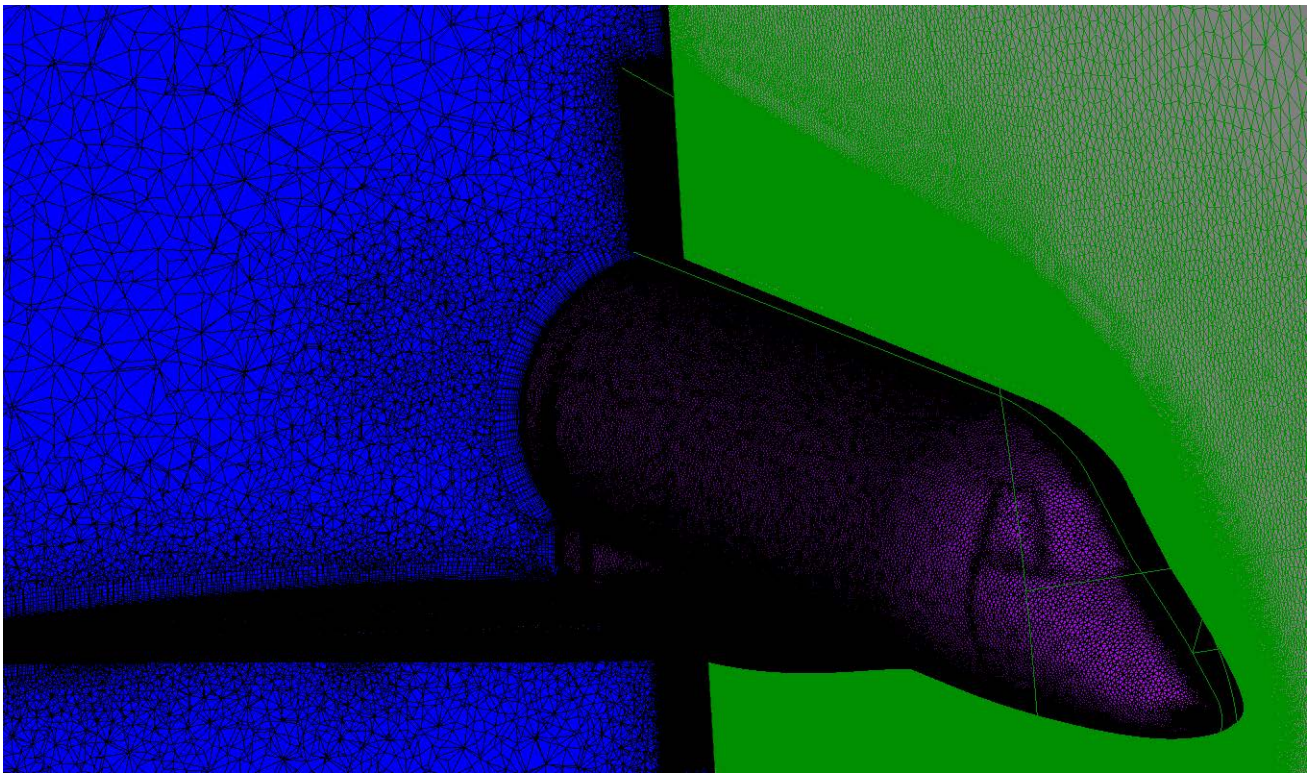

Figure 10: Surface and volume mesh distribution on and around the BRAC model.

6.0 FLOW SIMULATIONS AND APPROACH

All the flow simulations were performed on the NRC GPSC high performance computing cluster (160 computer nodes, each node having 16 Intel Xeon 2650v2 2.6-Ghz cores and 128 GB RAM) using the parallel Cobalt compressible flow solver on 200 processors. As an example of the processing speed, the full-

span configuration flow solution CPU rate was 44.6 seconds/timestep or 1.05 microseconds/cell/timestep. For each simulation, at least 6000 iterations were performed to ensure convergence and guarantee that there were sufficient aerodynamic load data sampling for averaging in case fluctuations were present.

The CFD investigation was conducted using the Cobalt compressible flow solver [8]. Fully turbulent flow simulations were performed using the Menter SST turbulence model [9] on a viscous unstructured grid. The four support peniche configurations (Baseline plus three alternates) were analysed and compared to the Reference (full-span) configuration in terms of aerodynamic loads and flow behaviour. The simulations were performed at Mach 0.2 at three angles of attack (α_1, α_2 and α_3).

The results in terms of surface pressure coefficient, vorticity and Mach number distributions, iso-surface vorticity, and aerodynamic load coefficients are presented and analysed for the freestream conditions given in Table 2. Following the wind tunnel reference, the coordinate system was defined such that the aircraft nose is located at (191.27, 0.0, 204.87) mm, with the balance centre at (1127.77, 0.0, 272.42) mm. For the aerodynamic loads, only the lift, drag and pitching moment coefficients were reported and processed to demonstrate the impact of the vertical tail configuration setup on the overall aerodynamic performance of the aircraft. The loads were integrated only on the portions of the model that would be mounted on the wind tunnel balance; the loads on the peniche, splitter plate, mirrored vertical tail and HStab extension were excluded.

6.1 Solution Convergence

All the simulations were performed using the Cobalt solver, which is based on a time-accurate global time-stepping scheme for which the time steps are specified in terms of the CFL number. Temporal convection and diffusion damping were considered to accelerate the convergence. All the solutions were marched in time until steady state was reached. Depending on the flow solution development through the iterative process, the global time step was varied until it reached a maximum value corresponding to a CFL number of 10^6. The flow solution yielded a y^+ value distribution close to unity or less, as shown in Figure 11, for the Baseline BRAC model, which conforms to the requirements of the Menter SST turbulence model considered in the present study.

An example of the time histories of the lift, drag and pitching moment coefficients for the Baseline BRAC model a given angle of attack (α_1) is illustrated in Figure 12. Overall, convergence was reached after the first 1000 iterations. However, the simulations were run for up to 6000 iterations for most configurations to ensure good convergence and accuracy in the loads increment among all BRAC configurations. The convergence of the solution was also monitored by considering the root mean square of the density and the turbulence model residuals, (DR/DT) and (DN/DT) respectively. As demonstrated in Figure 13, a four- and seven-fold drop was observed for the turbulence and density residuals, respectively, which is sufficient to guarantee solution convergence.

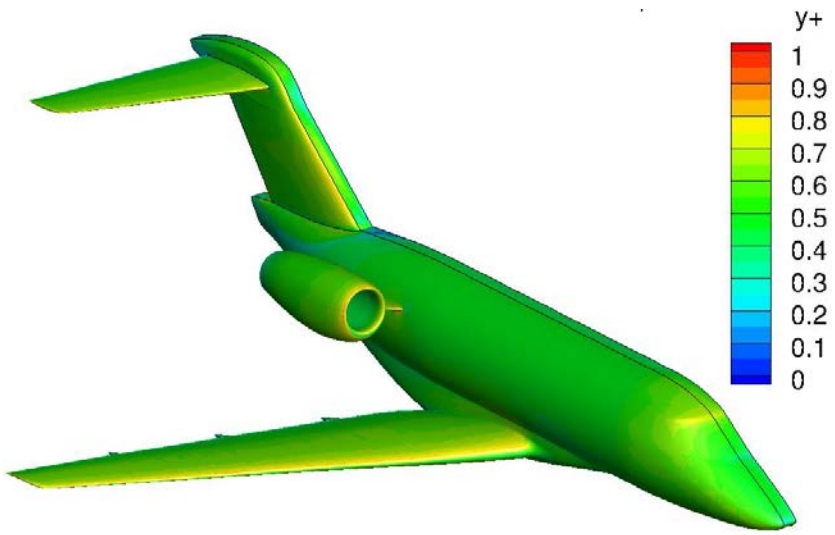

Figure 11: y^+ distribution off the BRAC model surface for a given angle of attack.

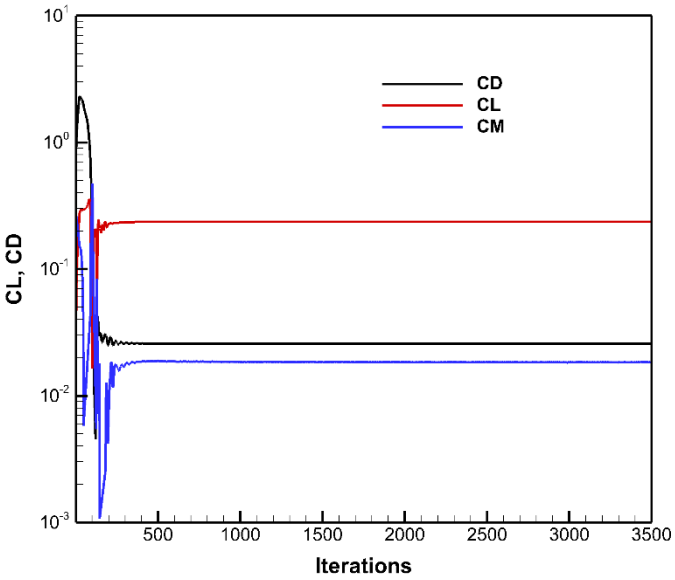

Figure 12: Convergence history of lift (CL), drag (CD) and pitching moment (CM) coefficients for a given angle of attack.

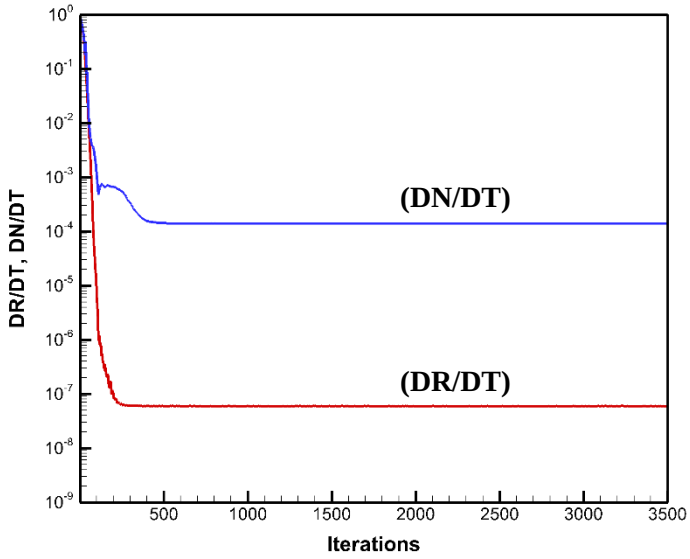

Figure 13: Convergence history of the root mean square of the density residual (DR/DT) and turbulence model residual (DN/DT).

6.2 Validation and Grid Sensitivity Study

In the wind tunnel, the boundary layer flow development for a half-model aircraft with a peniche and a splitter plate starts at the splitter plate leading edge. The boundary layer flow along the wind tunnel walls, which forms from the nozzle contraction and extends all the way to the test section, is diverted behind the splitter plate. Downstream of the splitter plate leading edge, the boundary layer becomes progressively thicker and the displacement thickness increases as we approach the peniche nose. An adverse pressure gradient starts to build up from the difference between the static and total pressures at the nose stagnation point, causing the boundary layer to separate. Therefore, the flow is forced to sink towards the splitter plate at the nose, forming a significant recirculation zone that gives birth to a well-formed vortical flow. Usually the recirculation, which causes an upstream flow on the splitter plate, separates again to form a secondary vortex. The combined vortices are stretched to form two distinct legs around the entire peniche length. They maintain their momentum all along the splitter plate and peniche until the upper arm impacts the vertical tail assembly. The vortices disrupt the flow considerably and may alter the true vertical tail and HStab aerodynamic loads, which compromise the half-model testing measurements (drag, lift and pitching moment coefficients).

A grid sensitivity study was performed for the present paper to assess the prediction quality of the horseshoe vortex formed on the splitter plate wall as the boundary layer impinges on the BRAC model peniche nose. The grid sensitivity study was also aimed to assess the accuracy of the overall aircraft aerodynamic load predictions against experimental data. To this end, the Baseline BRAC configuration, which consists of the half-model aircraft and a full peniche, was chosen for the grid sensitivity study and validation. Three mesh sizes were used: coarse, medium and refined. In all cases, the splitter plate was modeled as a non-slip boundary, and a horseshoe vortex was formed when the flow boundary layer impinges on the peniche nose. The medium mesh consisting of 47.5 million cells was judged adequate for predicting the aerodynamic loads of the BRAC model; however, the mesh was not designed to capture well the horseshoe vortex. The refined mesh consisting of 98.7 million cells was obtained by refining the grid on the lifting surfaces by a factor of 1.5 and adding a super-refined structured block designed to resolve the horseshoe vortex all the way from the fuselage nose to the vertical tail. Within the structured block, the grid crosswise resolution was about 0.5 mm at the nose and 1 mm elsewhere. The streamwise resolution was varied from 1 mm to 5 mm to reduce the cell count. A third coarse mesh consisting of 22 million cells was considered to complete the grid sensitivity

study. The coarse mesh was obtained from the medium mesh by removing all of the grid refinement sources (along the wing and HStab tip vortices, and along the wing, HStab and pylon wake refinement regions). On the BRAC model surfaces, the grid was coarsened by a factor of 2 while keeping the same spatial resolution at the leading and trailing edges of the wing and HStab.

The effect of grid resolution on the flow behaviour past the BRAC model and the tunnel splitter plate is displayed in Figure 14 in terms of the vorticity iso-surface (ω=500rd/s), which is a good indicator of the horseshoe vortex integrity and shape. Figure 14a shows the predicted horseshoe vortex around the BRAC model for a given angle of attack using the coarse mesh and Figure 14b shows medium mesh, which was not designed to capture the flow vortices accurately. Figure 14c illustrates the predicted horseshoe vortex using the refined grid along the vortex arms. For the coarse and medium meshes, the horseshoe vortex dissipates very quickly before reaching the BRAC vertical tail. The dissipation is so strong that the impact point on the vertical tail is shifted well upward. Also, the coarse mesh showed nearly fully dissipated wing and HStab tip vortices. However, the refined mesh showed a well-defined horseshoe vortex all the way from the peniche nose to the BRAC vertical tail, and along the BRAC belly.

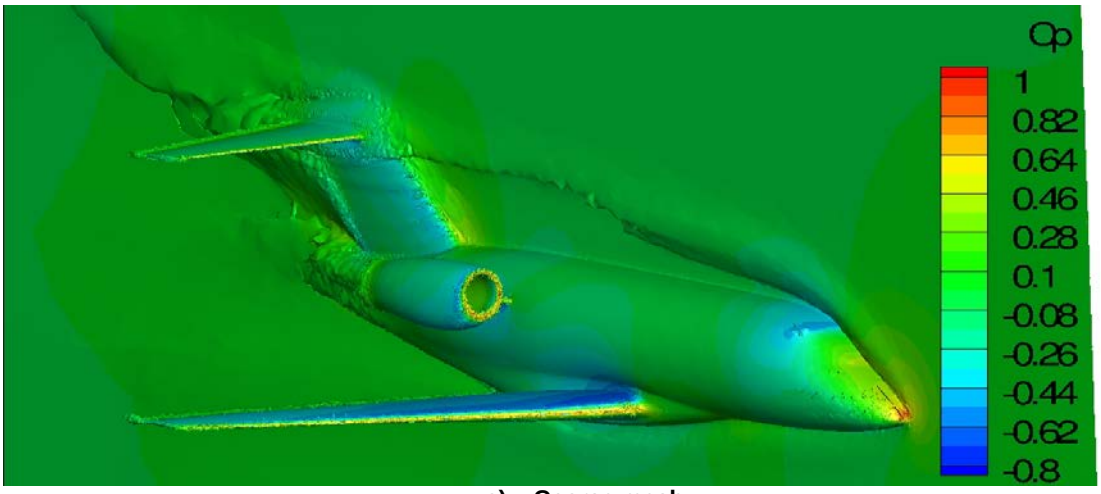

a) Coarse mesh

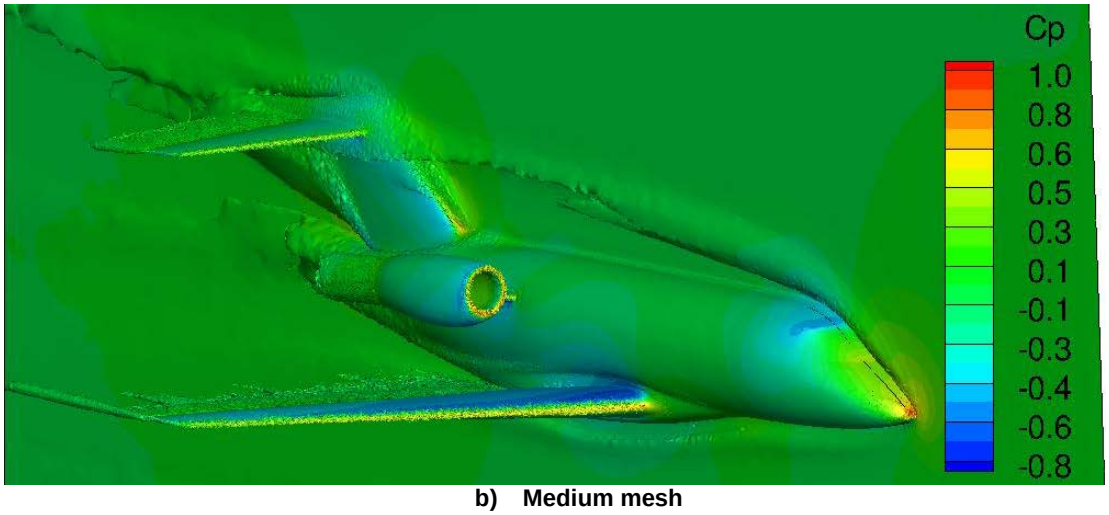

b) Medium mesh

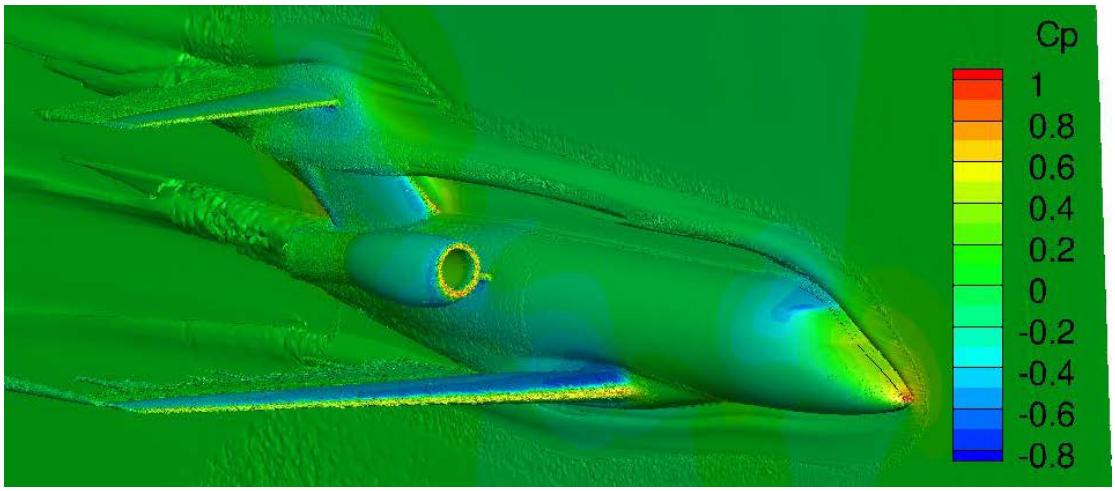

Refined mesh

Figure 14: Flow solution displayed in terms of the vorticity iso-surface (ω=500 rd/s) for the BRAC model with a full peniche, for a given angle of attack.

The boundary layer displacement thickness was computed 71.76 cm downstream from the splitter plate leading edge, where measurements were taken during the wind tunnel testing using pressure rake consisting of 20 Pitot tubes. For reference, the peniche nose was located at 59.39 cm. The measured and the computed boundary layer profiles are illustrated in term of the axial velocity U normalized with the freestream velocity Uinf in Figure 15. There is a slight discrepancy at the edge of the boundary layer, but otherwise the profiles match well. The CFD boundary layer profile was obtained with the fully turbulent flow assumption. However, in the experiment, a laminar boundary layer might be formed near the leading edge of the splitter plate before transitioning to fully turbulent boundary layer. The computed and measured velocity profiles yielded a boundary layer thickness (99% of the freestream velocity) of 8.7 mm and a boundary layer displacement thickness of 1.2 mm. Therefore, the peniche thickness is about 3 times the thickness of the boundary layer and 21 times the displacement thickness of the boundary layer. The analytical turbulent boundary layer profile computed with the 1/7 exponent yields a displacement thickness of 1.3 mm. Another boundary layer profile is displayed at a distance of 240.26 cm (on the top of the vertical tail) downstream of the splitter plate leading edge where the computed boundary layer thickness is 2.56 cm, which corresponds to the peniche thickness.

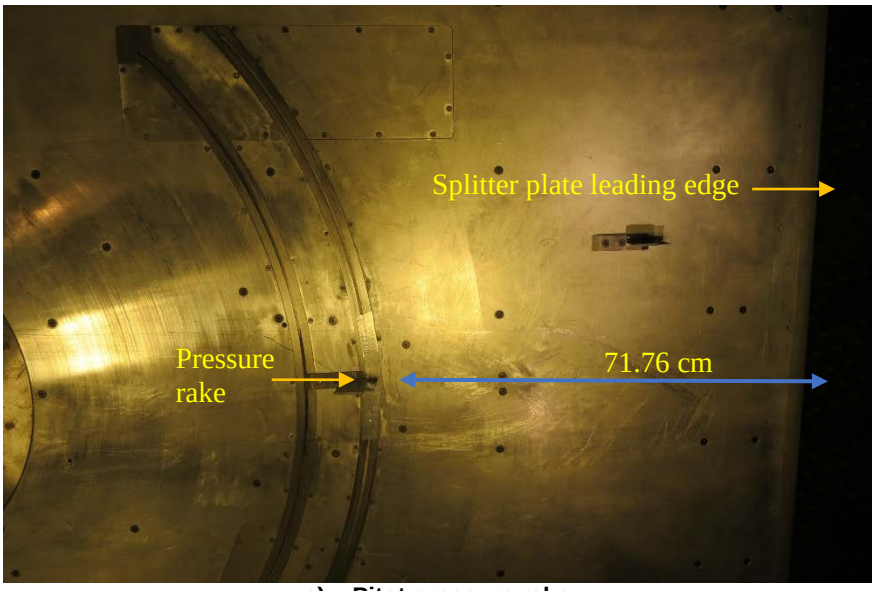

a) Pitot pressure rake

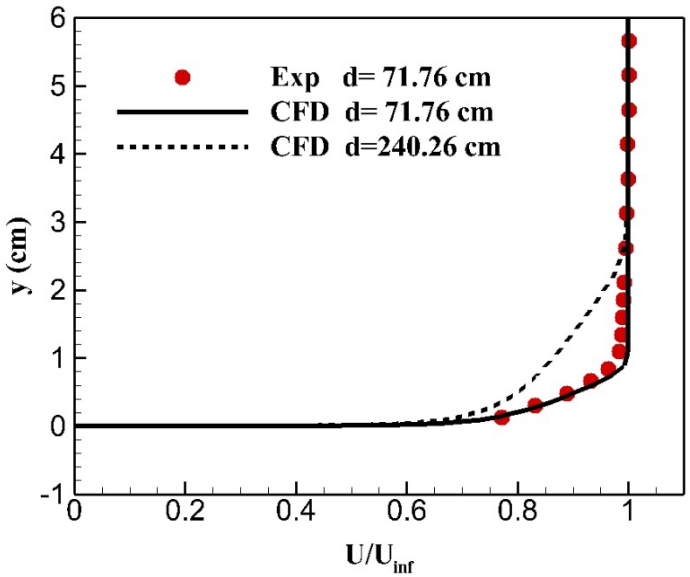

b) Measured and computed velocity profiles

Figure 15: Measured and computed velocity profiles at distances d from the splitter plate leading edge.

To validate the CFD predictions against experimental data, the Baseline BRAC configuration (2-D full peniche) was modelled at three angles of attack. The CFD simulations were performed with a no-slip condition boundary on the splitter plate surface, at the same Mach and Reynolds numbers as run in the tunnel, and with free-air conditions imposed at the farfield boundaries as described previously. The wall ahead of the splitter plate was treated as a slip wall. The resulting load data were then compared to the half-model wind tunnel data corrected for the three farfield walls. Figure 16 shows a graphical comparison between the CFD results and the measured data. The Reference (full-span) model CFD data are also included to quantify the half-model support effect. Excellent agreement was obtained for the Baseline lift, drag and pitching moment coefficients for Mach 0.2 at three angles of attack. The predicted aerodynamic loads of the

coarse, medium and refined mesh cases are depicted (for α1 only) in the graphs by a purple diamond, green circle and solid square symbols, respectively. Despite the large differences between the three mesh sizes (22 to 99 million cells), the three CFD data points are all close to the experimentally measured data. The most important aspect of the grid sensitivity study is to show that the solution tends to show a converging trend while refining the mesh. Also, it is worth mentioning that the experimental data are not necessarily the ideal "truth" as errors can be present during the experiment (including measurement and data correction errors), which are difficult to quantify. Therefore, refining the grid does not necessarily mean that the CFD will converge towards the experimentally measured data. There are also errors associated with the CFD simulations (e.g., due to turbulence models and numerical schemes). However, from engineering point of view, the high-fidelity CFD results and the measured data are at an acceptable level of agreement, suggesting that the CFD is accurate enough for studying alternate half-model mounting configurations.

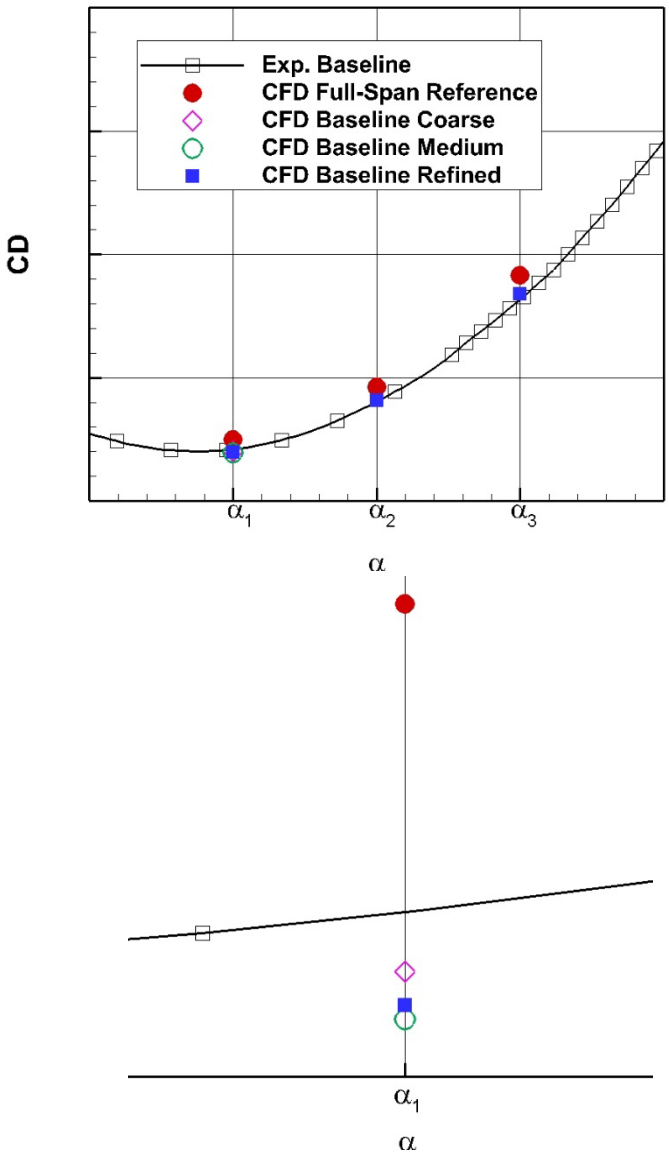

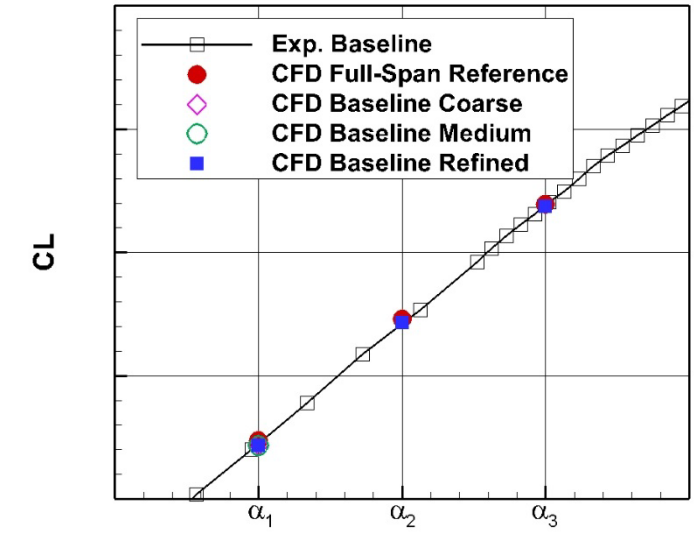
Exp. Baseline
CFD Full-Span Reference
CFD Baseline Coarse
CFD Baseline Medium
CFD Baseline Refined
CL
α1
α2
α3
α

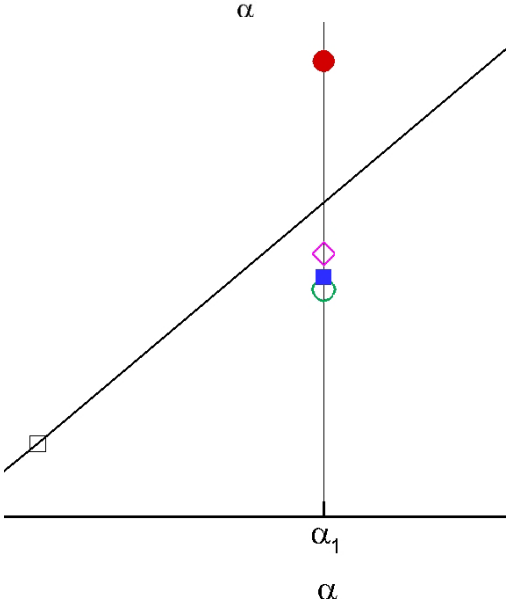
α1
α

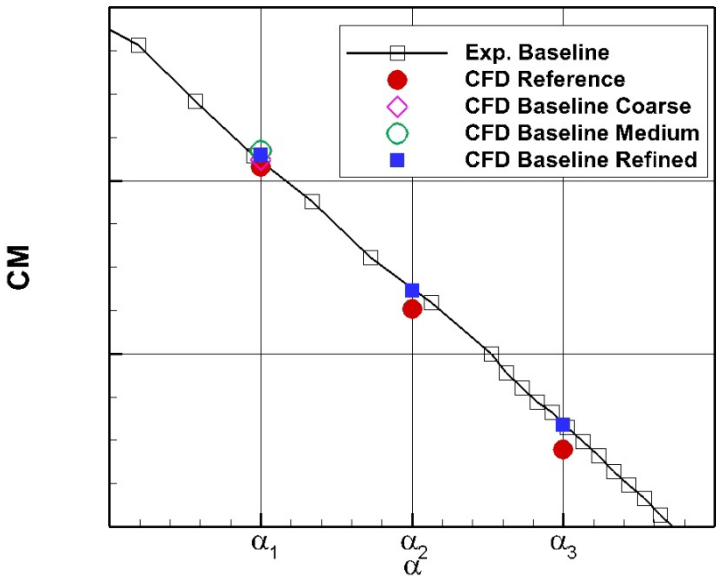
Exp. Baseline
CFD Reference
CFD Baseline Coarse
CFD Baseline Medium
CFD Baseline Refined
CM
α1
α2
α3
α

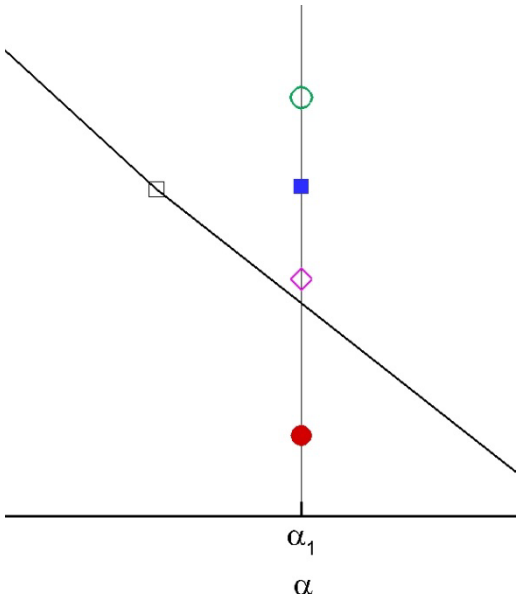

Figure 16: Comparison of the CFD results and the experimental data for the BRAC drag, lift and pitching moment coefficients, with enlargements provided for α_1.

7.0 DATA ANALYSIS AND DISCUSSION

In the present analysis, the focus is the effect of the splitter plate horseshoe vortex flow on the overall aerodynamic performance of the BRAC model with its T-tail arrangement. The presence of the boundary layer flow on the splitter plate and the resulting horseshoe vortex structure in the tunnel makes it difficult to achieve the goal of obtaining a flow field identical to the full-span representation. The peniche used for the Baseline configuration was intended to reduce the impact of the reflection plane boundary layer flow and the horseshoe vortex, but it creates a significant flow alteration around the BRAC vertical tail where the flow physics are completely different from the full-span configuration. This obviously contaminates the measured data and compromises the overall measured aerodynamic performance of the vehicle to some extent.

Note that all results presnted below made use of the refined grid mesh.

7.1 Flow Structure

Figure 17 shows the horseshoe vortex formation near the fuselage nose, which is then convected downstream below and above the BRAC model centerline until it reaches the vertical tail assembly, where it interacts with other induced vortical flows. To illustrate this flow behaviour, streamlines were seeded in the simulation data right across the cores of the vortices to track their paths, as displayed in Figure 18. Near the peniche nose, Figure 18b, the birth and formation of the primary and secondary horseshoe vortices is observed, which is clearly depicted in Figure 18c by the vorticity magnitude distribution on a cutting plane through the peniche nose. The lower arm of the horseshoe vortex is convected downstream below the BRAC model peniche, and does not have a significant impact on the measured model aerodynamics. The upper arm, however, follows the peniche outline as it heads towards the vertical tail assembly, where it is combined with other flow vortices, as displayed in Figure 18d. The splitter plate boundary layer causes vortical flow along the leading edge of the vertical tail, where it is convected upwards and then downstream on top of the bullet-

shaped fairing. The boundary layer also causes the formation of a horseshoe vortex at the root of the vertical tail, which is then convected downstream along the tail. Owing to flow separation at the trailing edge of the vertical tail, a funnel vortex is formed behind the peniche, which is sucked upwards to merge with the primary horseshoe vortex. This flow behaviour may cause a decrease in the static pressure and change the flow patterns past the vertical tail and the HStab. All of these vortices create complex flow patterns past the vertical tail. Therefore, it was thought that introducing a gap between the vertical tail and the splitter plate might clean up the region and make the flow more streamlined.

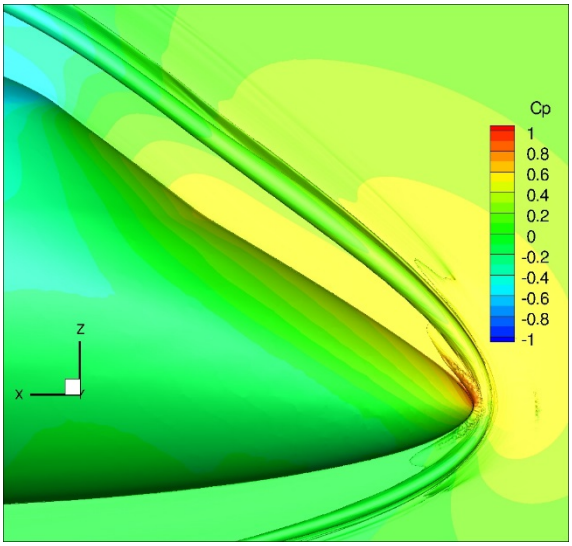

a) Nose region horseshoe vortex (ω=5000 rd/s iso-surface)

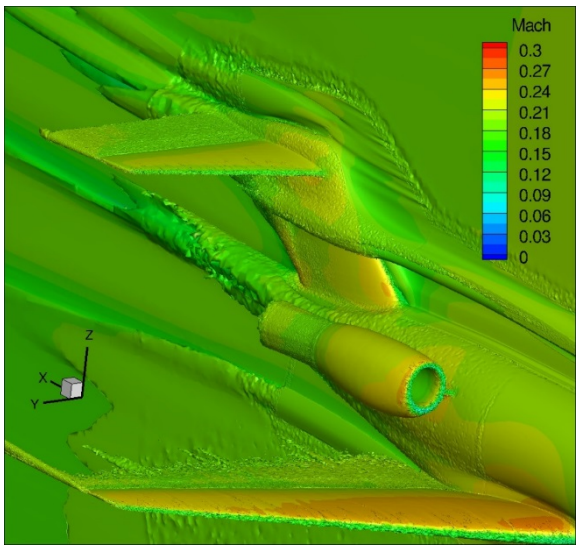

b) Flow vortices past the vertical tail (ω=600 rd/s iso-surface)

Figure 17: Flow vortex system past the BRAC model at low angle of attack. The vorticity iso-surface is flooded with the a) pressure coefficient and b) Mach number distributions.

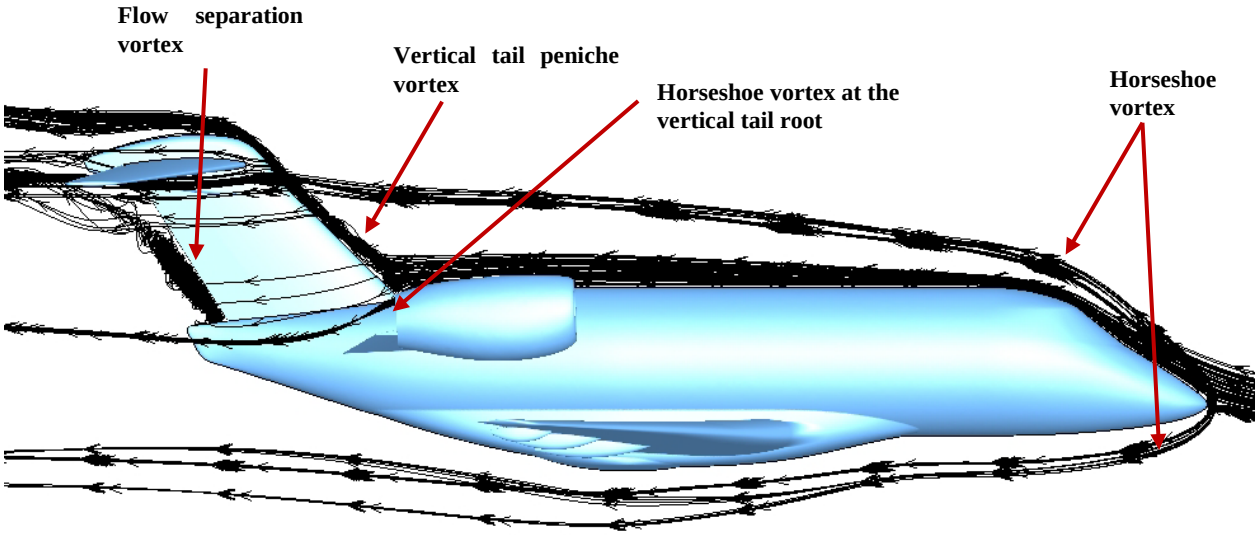

a) Overview of the vortex system

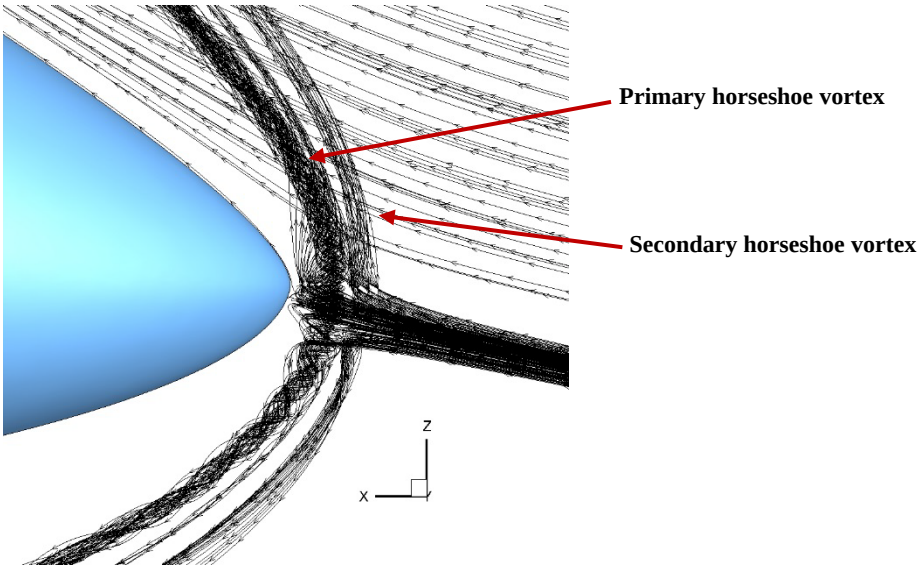

b) Horseshoe vortex formation near the peniche nose

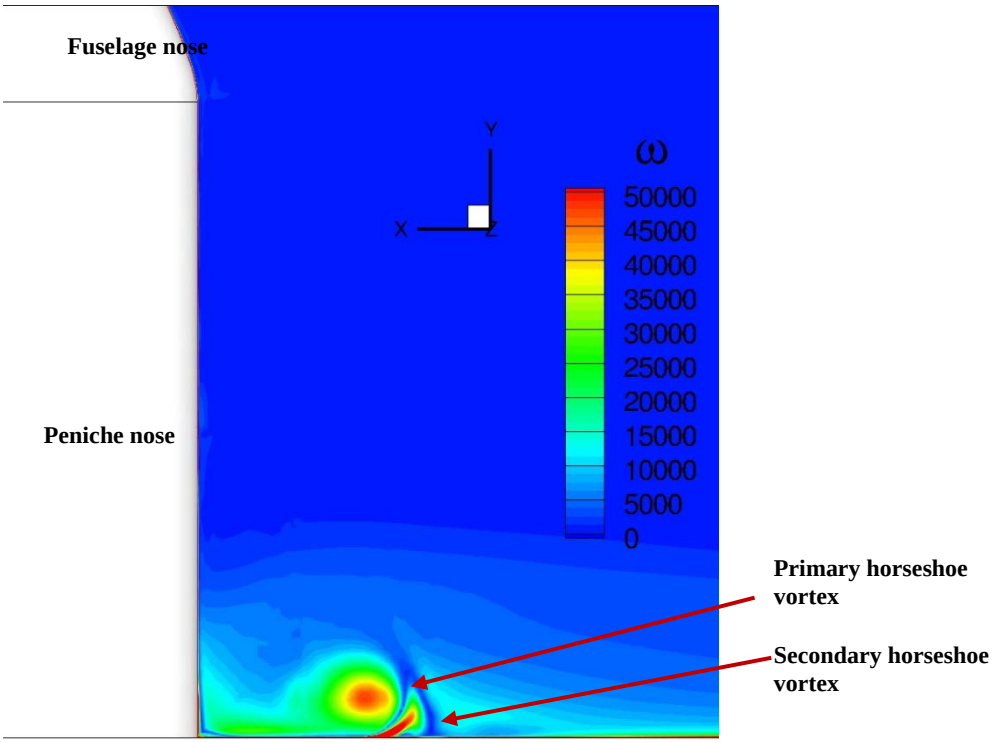

c) Horseshoe vortex core near the peniche nose

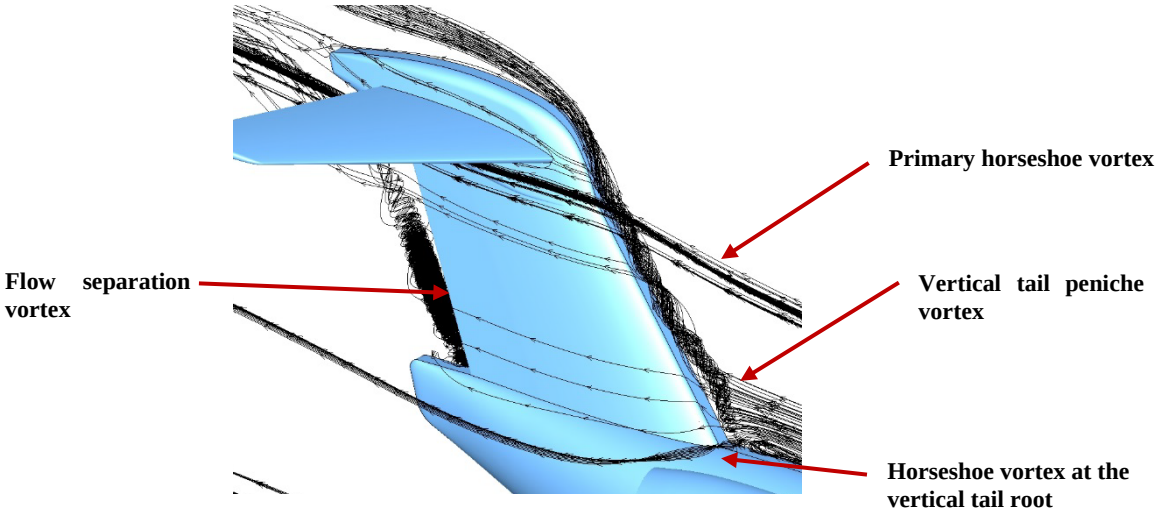

d) Vortex system past the vertical tail

Figure 18: Flow vortices system past the Baseline BRAC model in terms of streamlines at high angle of attack.

Figure 19 exemplifies the horseshow vortex structure past the Baseline BRAC model at various angles of attack. At low angle of attack, the horseshoe vortex impinges on the vertical tail at mid-height. As the angle of attack increases, the impingement point move towards the bullet-shaped fairing. Figure 20 shows a close-up view of the vortex system past the vertical tail assembly for various angles of attack. The vortex system around the ALT1 configuration, which was introduced to create a gap between the vertical tail base and the

splitter plate in an attempt to improve the flow behaviour around the vertical tail, is shown in Figure 21. The primary vortex structures are similar: the path of the horseshoe vortex does not change, and the vortex is split at the vertical tail leading edge, passing inside the gap and around the vertical tail. This prevents the flow from mimicking full-span flow conditions. However, owing to the curved vertical tail leading edge compared to the blunt edge of the peniche, the secondary horseshoe vortex at the root of the tail is weakened significantly, if not mitigated completely, improving the flow behaviour in the tail region.

Figure 22 illustrates the horseshoe vortex encounter with the top of the vertical tail bullet for all configurations. As discussed earlier, the Baseline BRAC configuration displays a very complex flow structure around the vertical tail tip region, see Figure 22a. Creating a gap between the vertical tail base and the splitter plate helps to streamline the flow and eliminates some vortex structures found with the Baseline model, see Figure 22b-d for the ALT1, ALT2 and ALT3 configurations, respectively. Note that ALT3, which has a vertical tail with a bullet-shaped fairing, induced a flow behaviour closer to full-span situation and that is better than the ALT1 and ALT2 configurations do. However, for all three alternate configurations, the horseshoe vortex gets split at the vertical tail, causing the flow to pass through the gap and around the tail, see Figure 23 (only ALT1 shown; the flow is similar for ALT2 and ALT3).

Adding the bullet-shaped fairing and HStab extension in the gap creates some blockage. Therefore, it is surmised that the peniche thickness must be increased slightly to contain the horseshoe vortex within the gap and shield the starboard side of the vertical tail from the horseshoe vortex flow.

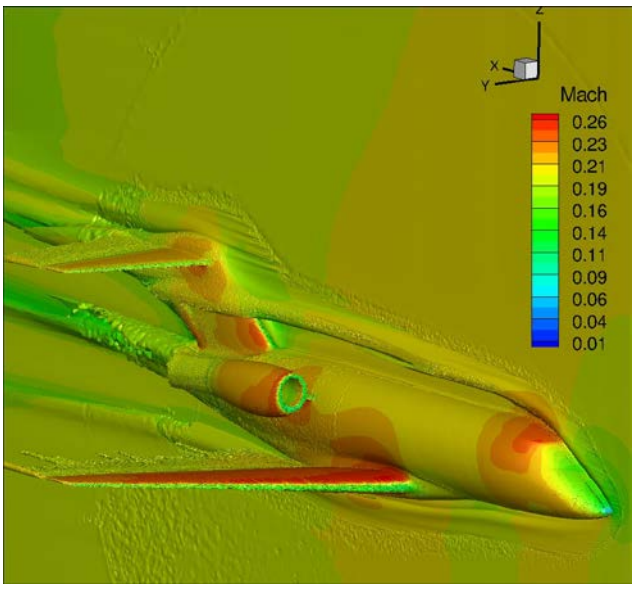

a) Low pitch angle

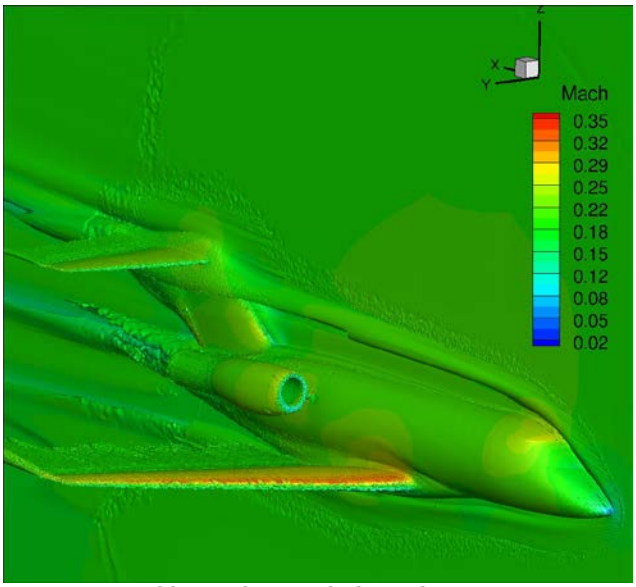

b) Moderate pitch angle

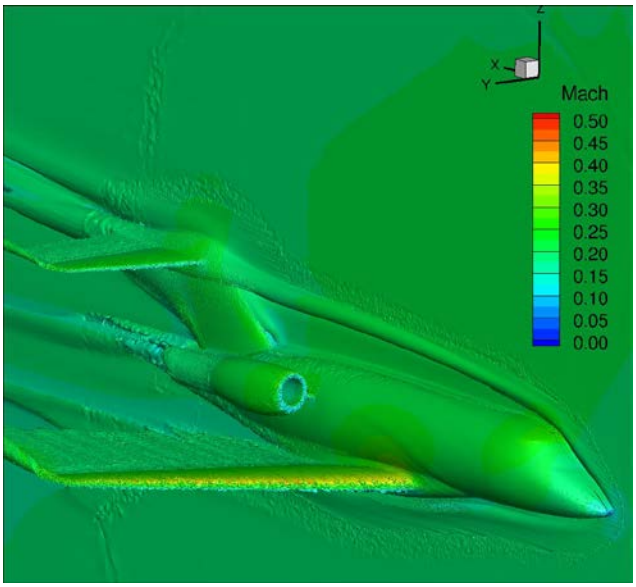

c) High pitch angle

Figure 19: Horseshoe vortex path around the Baseline BRAC model for different pitch angles, depicted with ω=600 rd/s vorticity iso-surface.

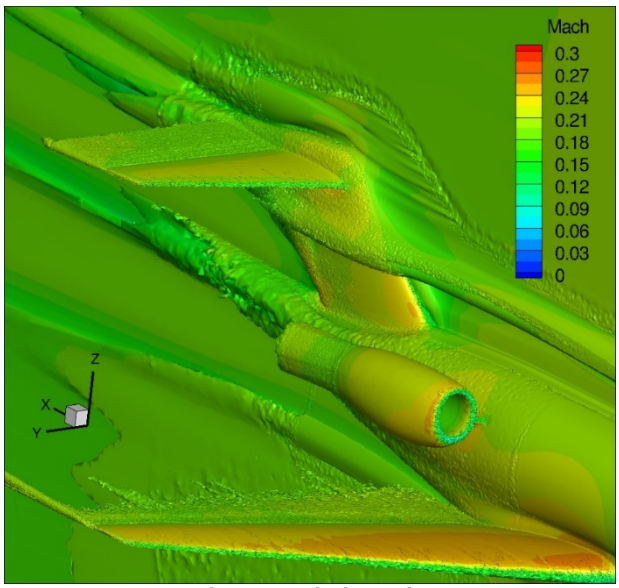

a) Low pitch angle

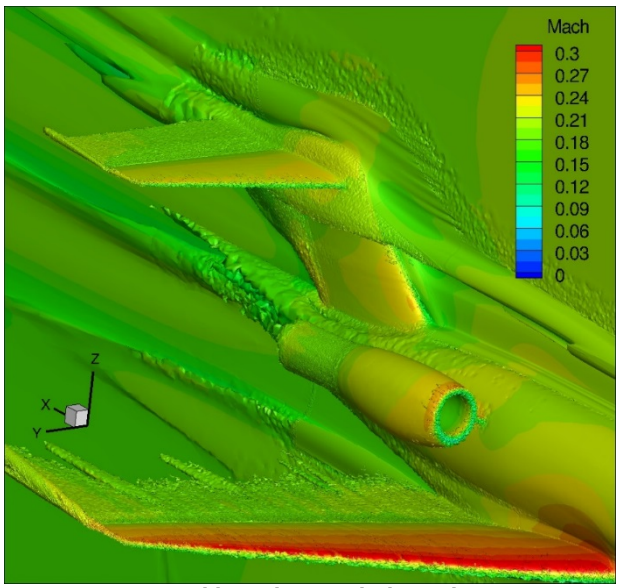

b) Moderate pitch angle

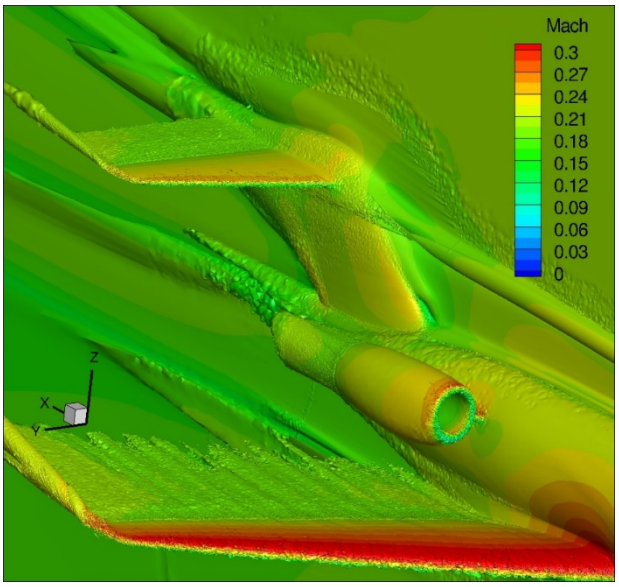

c) High pitch angle

Figure 20: Close-up view of the flow vortex system past the Baseline BRAC model vertical tail at different pitch angles, depicted with ω=600 rd/s vorticity iso-surface.

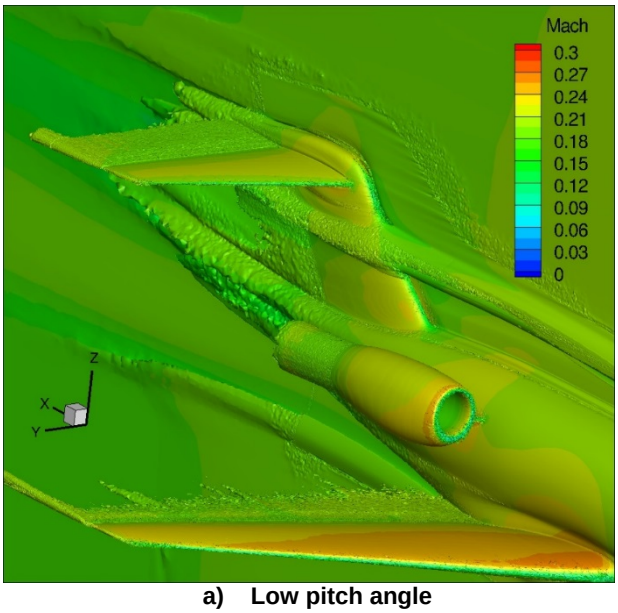

a) Low pitch angle

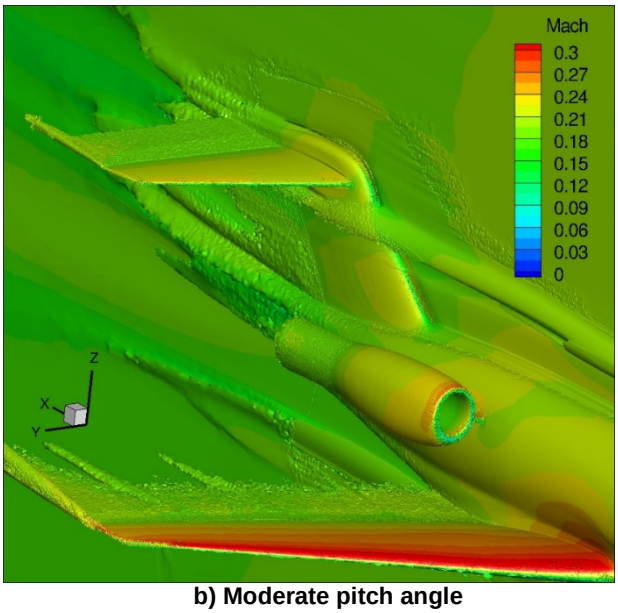

b) Moderate pitch angle

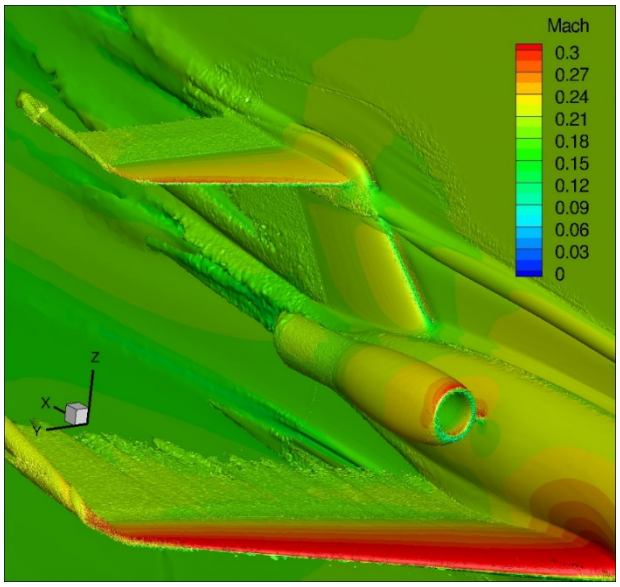

c) High pitch angle

Figure 21: Close-up view of the flow vortex system past the ALT1 BRAC model vertical tail at different pitch angles, depicted with ω=600 rd/s vorticity iso-surface.

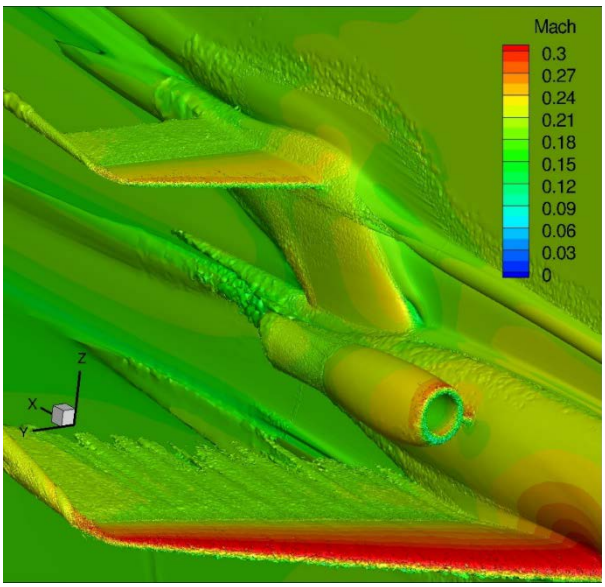

a) Baseline

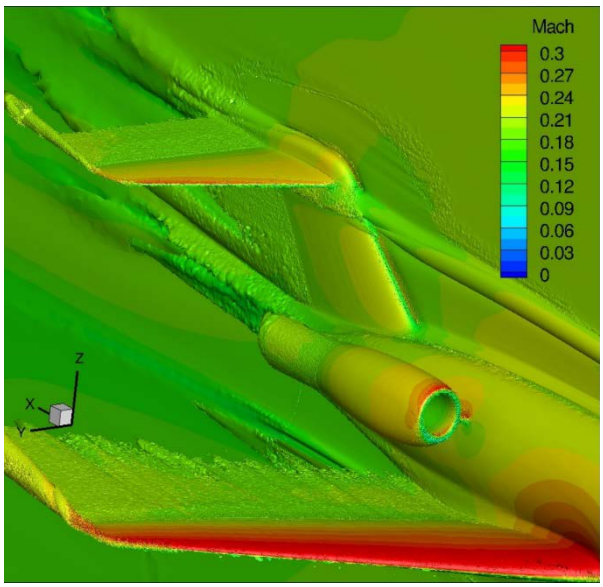

b) ALT1

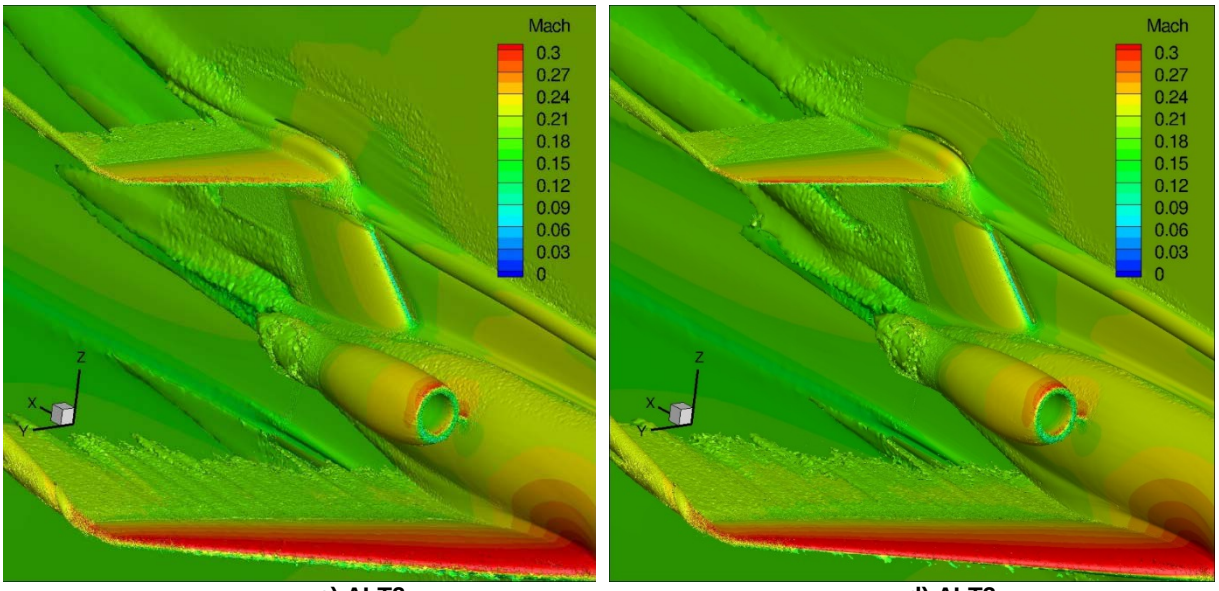

c) ALT2 d) ALT3

Figure 22: Close-up view of the flow vortex system past the BRAC model vertical tail at high pitch angles, depicted with ω=600 rd/s vorticity iso-surface.

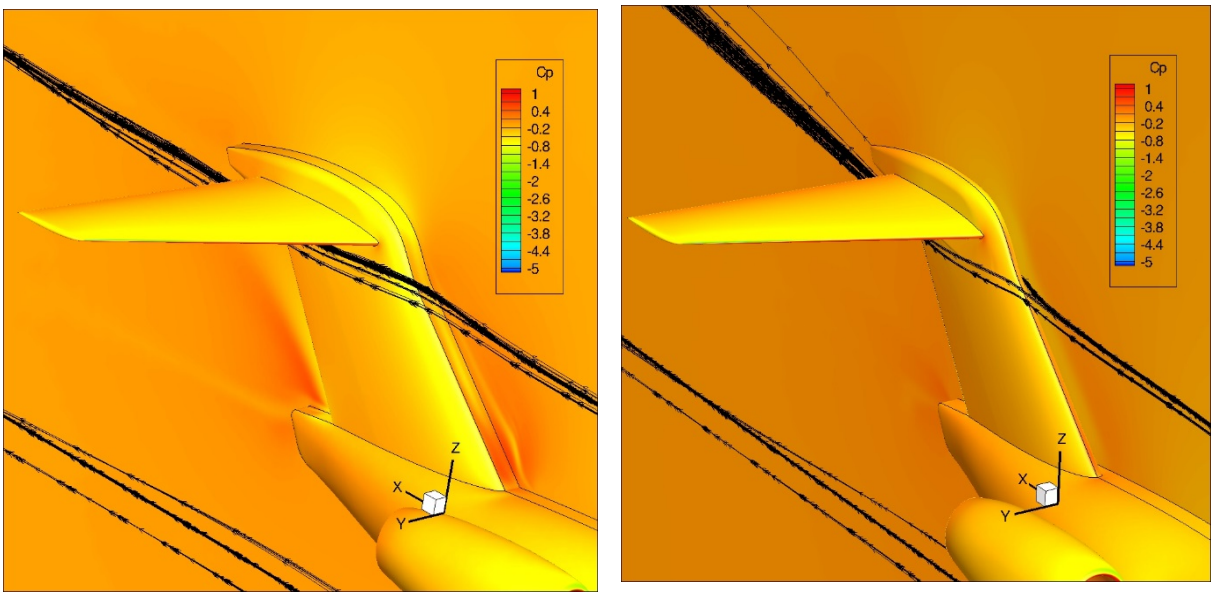

a) Baseline b) ALT1

Figure 23: Close-up view of the flow vortex system in terms of streamlines past the Baseline and ALT1 BRAC model vertical tails at high pitch angles.

7.2 Aerodynamic Loads

The main objective of the present CFD analysis is to determine the best vertical tail set-up in the wind tunnel that will make measurements with the HStab installed useful and reliable for aircraft design and certification. Within this context, the best configuration would be the one with wind tunnel aerodynamic performance closest to the full-span model. Therefore, a comparison between the aerodynamics of the four configurations was performed at subsonic conditions in terms of the drag, lift and pitching moment coefficient increments

relative to the Reference full-span configuration.

The drag (CD), lift (CL) and pitching moment (CM) increments for each configuration are defined as follows:

$$\begin{aligned} \Delta CD &= CD_i - CD_{Ref} \\ \Delta CL &= CL_i - CL_{Ref} \\ \Delta CM &= CM_i - CM_{Ref} \end{aligned} \tag{1}$$

where i=Baseline, ALT1, ALT2 and ALT3 for the Baseline and the three alternates, and the subscript *Ref* denotes the Reference full-span configuration.

Starting with the overall BRAC aerodynamic force coefficient increments, as shown in Figure 24, all the alternate configurations yield improved (reduced) increments relative to the Reference full-span model; the increments are reduced by at least 50% in lift and drag relative to the Baseline model, although surprisingly, there was no improvement in the pitching moment increments. All three alternate configurations with a gap at the vertical tail behave similarly and the differences between each are likely within the error bounds of the analysis.

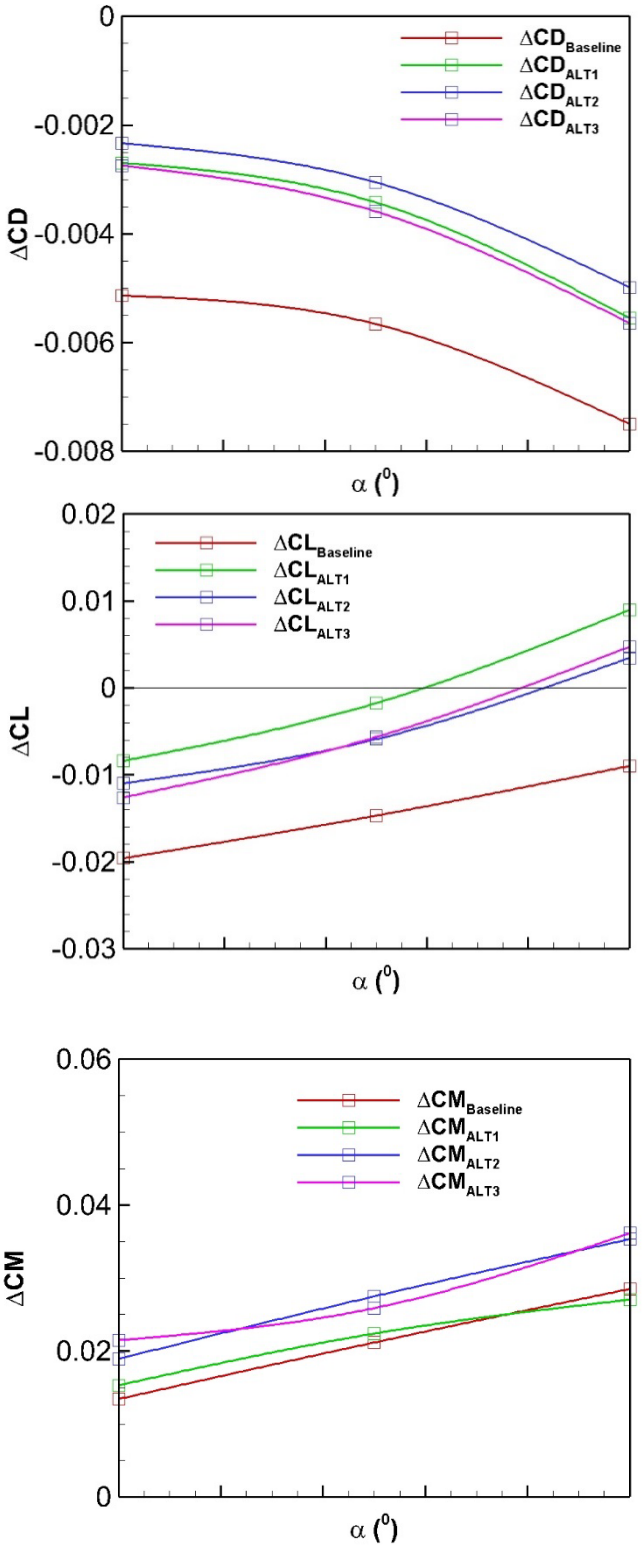

Figure 24: Overall BRAC model drag, lift and pitching moment coefficient increments for the Baseline and three alternate configurations with respect to the Reference full-span configuration.

Another way to illustrate the aerodynamic outcome of the three alternates is to consider uniquely the loads on the HStab. This is presented in Figure 25, which shows the HStab load increments with respect to the Reference full-span configuration. The aerodynamic coefficients were obtained using the reference flow conditions, length and area depicted in Table 2. These results show a clear benefit in the Hstab drag coefficient contribution for the configurations with the gap between the vertical fin and the splitter plate; however, a similar grouping of curves was not apparent for the HStab contributions to the lift or pitching moment increments. In general, the ALT1 configuration provided HStab coefficients that were closest to the full-span Reference case.

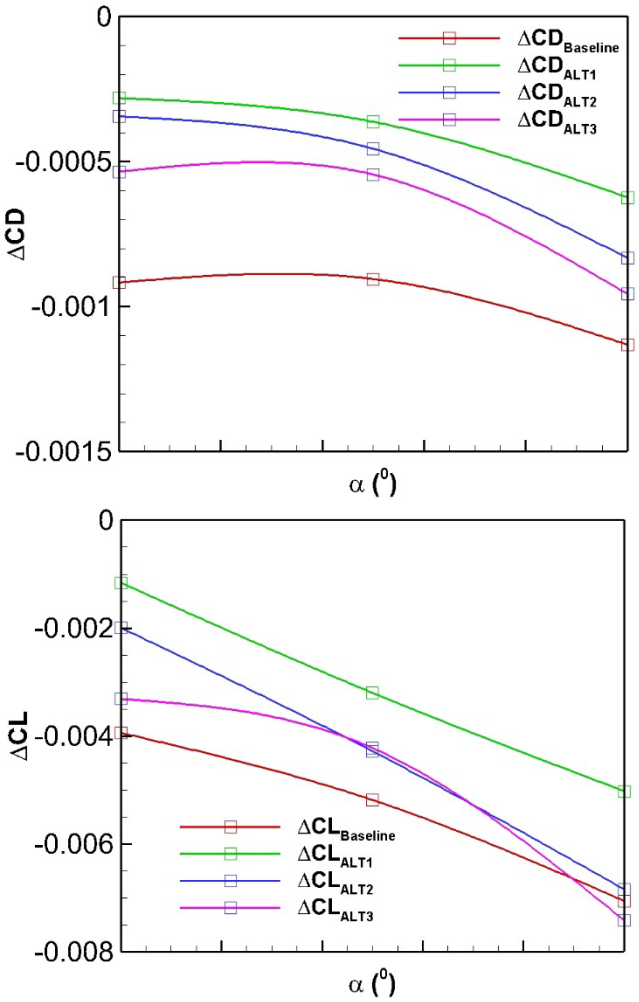

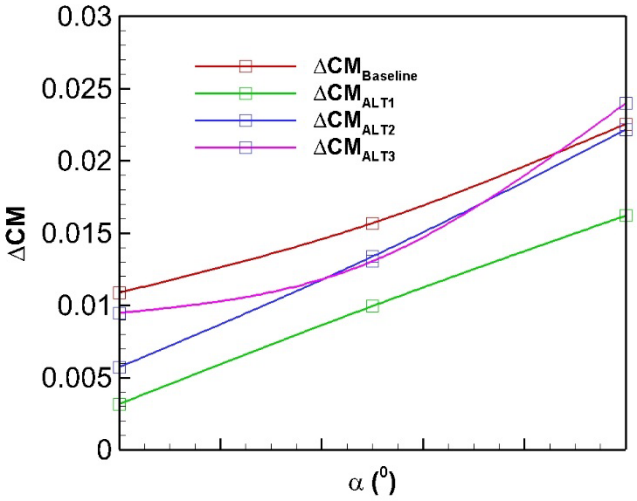

Figure 25: Overall BRAC HStab drag, lift and pitching moment coefficient increments for the Baseline and the three alternate configurations with respect to the Reference full-span configuration.

8.0 CONCLUSION

A CFD investigation was performed to assess the impact of the support interference of an actual and several proposed BRAC half-models with vertical T-tails in the wind tunnel. Several flow conditions were considered, corresponding to wind tunnel measurement data points at Mach 0.2 and three angles of attack. The objective of this project was to determine the best half-model vertical T-tail setup that leads to aerodynamic loads that are similar to those obtained with the ideal full-span configuration. The experimental wind tunnel measurement data for the Baseline half-model installation configuration were corrected for the farfield wall interference using standard methodology. All CFD simulations were performed with free-air farfield boundary conditions. Four vertical T-tail setup configurations were considered and compared to each other and the ideal full-span configuration in terms of aerodynamic loads and flow patterns. The flow simulations were performed on viscous unstructured grids using the Menter SST turbulence model.

The Baseline CFD results compared well with the wind tunnel measurement data. Therefore, we expect that the CFD results obtained for the other configurations are quite reliable for predicting the flow physics and the impact of the support interference on the BRAC model aerodynamic performance. Since wind tunnel modifications are expensive to make, CFD analyses are a cost-effective means for reducing half-model support interference. The flow solutions obtained for the four configurations investigated in the present paper did not exhibit substantial time fluctuations. Therefore, the Menter SST turbulence model was judged to be adequate for this work. The use of higher fidelity CFD simulations with more advanced turbulence modelling (such as large eddy simulations or hybrid turbulence models) is not expected to bring about significant improvements to the quality of the flow predictions.

A refined dense grid was used to capture the vortical flows past the BRAC model. As expected, a horseshoe vortex was formed on the wind tunnel splitter plate, induced by the splitter plate boundary layer interaction with the BRAC model peniche nose. The upper arms of the horseshoe vortex were convected downstream, without losing significant momentum, and impacted the leading edge of the vertical tail. The impact position was seen to move upward along the vertical tail as the angle of attack was increased. For the Baseline configuration with a 2D full peniche, other vortical flow systems were seen to form around the vertical tail

assembly, such as a small horseshoe vortex at the vertical tail root, vortical flow along the vertical tail peniche and a twisting vortex behind the vertical tail trailing edge. Creating a gap between the vertical tail base and the splitter plate improved the flow field and eliminated the vortical flow observed in the gap, although the primary horseshoe vortex continued to impact the vertical tail leading edge. Probing the boundary layer characteristics at a location close to the fuselage nose indicated that the peniche height was 3 times the height of the boundary layer thickness and 21 times the displacement thickness. However, the boundary layer thickness grew as the flow passed over the aircraft so that it was equal to the peniche thickness at the vertical tail. Further simulations are required to determine whether it is more important to have a thick enough peniche so that the tail remains outside of the boundary layer, or whether a thinner peniche leading to a reduced horseshoe vortex at the nose of the model would be beneficial. Although the literature review indicated that some half models tested without a peniche had reduced support interference effects, these models did not have a tail.

Overall, the BRAC aircraft T-tail model with a fuselage peniche and a gap between the vertical tail and the wind tunnel wall reflection plate, without a bullet-shaped fairing or extended HStab on the vertical tail, was found to be the most promising configuration out of the proposed options. More flow simulations are planned to investigate other model configurations that may reduce or mitigate the horseshoe vortex that is induced by the wind tunnel test section splitter plate boundary layer as it interacts with the model peniche. Once an ideal configuration is determined, the CFD results will be validated by a wind tunnel test. The results of this investigation will serve as a guide for future BRAC model design modifications, leading to reduced support interference for half-models during wind tunnel testing.

9.0 ACKNOWLEDGMENT

The authors would like to acknowledge the support of Bombardier Aerospace, and in particular, thank Dr. Farzad Mokhtarian and his team for providing the BRAC CAD model and for helping with the design of the various BRAC alternate models. The authors would like also to thank Dr. Stuart McIlwain for reviewing this paper thoroughly and for very fruitful discussions.

REFERENCES

[1] Milholen, W.E., and Chokani, N., “Development of semi-span model test techniques”, AIAA 96-2412, 14th AIAA Applied Aerodynamics Conference, 17-19 June 1996, New Orleans, LA, USA.

[2] Doerffer, P., and Szulc, O. (2006), “High-lift behaviour of half-models at flight Reynolds numbers”, TASK Quarterly : Scientific Bulletin of Academic Computer Centre in Gdansk, Vol. 10, No 2**,** 2006 pp. 191-206.

[3] Eder, S., Hufnagel, K., and Tropea, C. (2006), “Semi-span testing in wind tunnels”, 25th International Congress of the Aeronautical Sciences, 3-8 September 2006, Hamburg, Germany.

[4] Yokokawa, Y., Murayama, M., Uchida, H., Tanaka, K., Ito, T. and Yamamoto, K. (2010), “Aerodynamic influence of a half-span model installation for high-lift configuration experiment”, 48th AIAA Aerospace Sciences Meeting Including the New Horizons Forum and Aerospace Exposition, January 2010, Orlando, Florida, USA.

[5] Skinner, S. N. and Zare-Behtash, H. (2017), “Semi-span wind tunnel testing without conventional peniche”, Exp Fluids (2017) 58:163 https://doi.org/10.1007/s00348-017-2442-7

[6] Chan, D.T., Hooker, J.R., Wick, A.T., Plumley, R., Zeune, C., Ol, M. V., and DeMoss, J.A. (2017), "Transonic semi-span aerodynamic testing of the hybrid wing body with over wing nacelles in the National Transonic Facility", 55th AIAA Aerospace Sciences Meeting, AIAA SciTech Forum, (AIAA 2017-0098), 9 - 13 January 2017, Grapevine, Texas, USA.

[7] Wick, A.T., Hooker, J.R., Walker, J., Chan, D.T., Plumley, R., and Zeune, C. (2017), "Hybrid wing body performance validation at the National Transonic Facility", 55th AIAA Aerospace Sciences Meeting, AIAA SciTech Forum (AIAA 2017-0099), 9 - 13 January 2017, Grapevine, Texas, USA.

[8] Cobalt Solution Inc., https://www.cobaltcfd.com/

[9] Menter, E. (1994), "Two-Equation Eddy-Viscosity Turbulence Models for Engineering Applications", AIAA Journal, Vol. 32, August 1994, pp. 1598-1605.

[10] Pointwise, http://www.pointwise.com

[11] Broughton, C.A., Benmeddour, A., Mébarki, Y., and Rivers, M.B. (2018), “Experimental investigations of the NASA common research semispan model in the NRC 5-Foot Trisonic Wind Tunnel”, AIAA AVIATION Forum, June 25-29, Atlanta, Georgia, 2018, DOI: 10.2514/6.2018-4285.

[12] Mokry, M (2006), “Subsonic Wall Corrections in the 1.5 M Wind Tunnel”, Laboratory report, LR-AL-2006-0056, NRC Institute for Aerospace Research, Ottawa, Canada, April 2006.